Title
A CLOUD CHAMBER INVESTIGATION OF LOW ENERGY RANGE ENERGY RELATION

Author
Mills, Robert Gail.

Publication Date
1952-05-13

UNIVERSITY OF CALIFORNIA — BERKELEY

RADIATION LABORATORY

DISCLAIMER

UCRL-1815
Unclassified-Physics Distribution

UNIVERSITY OF CALIFORNIA

Radiation Laboratory

Contract No. W-7405-eng-48

A CLOUD CHAMBER INVESTIGATION OF LOW ENERGY RANGE-ENERGY RELATIONS

Robert Gail Mills

(Thesis)

May 13, 1952

Berkeley, California

TABLE OF CONTENTS

A CLOUD CHAMBER INVESTIGATION OF LOW ENERGY RANGE-ENERGY RELATIONS

Robert Gail Mills

Radiation Laboratory, Department of Physics
University of California, Berkeley, California

May 13, 1952

ABSTRACT

An expansion cloud chamber has been developed which operates at a pressure before the expansion in the region of 45 millimeters of mercury. This chamber has been applied to the investigation of the range-energy relations for protons, alpha particles, and oxygen ions in the kilovolt region using elastic recoils from monoenergetic neutrons.. These curves are presented. A discussion of the chamber and general considerations in the design of low pressure cloud chambers are included.

A CLOUD CHAMBER INVESTIGATION OF LOW ENERGY RANGE-ENERGY RELATIONS

Robert Gail Mills

Radiation Laboratory, Department of Physics
University of California, Berkeley, California

May 13, 1952

PART ONE: RANGE-ENERGY RELATIONS AT LOW ENERGIES

Chapter One

Experimental Results

1.1 Previous Work. The behavior of low energy charged particles in the kilovolt region in passing through matter is complicated by the continually changing charge present on the particle. At higher energies the particle does not pick up or lose electrons, but when its velocity has been reduced to the region of orbital electron velocities, the total charge of an ion fluctuates rapidly. An adequate theory giving the effective mean charge of an ion near the end of its path has not been developed, although Bohr has investigated the problem of the total range of fission fragments.[1] Since fission fragments have both large nuclear charges and masses, they include a large part of their entire path length in the velocity region of variable charge. Bohr adopts a model of the process in which the total charge either remains constant or decreases. He defines the electron core to be that collection of electrons which in a neutral atom would have velocities greater than the velocity of the fission fragment. He then assumes that the ion carries only the core, i.e.,

the atom sheds an electron as soon as the atom's velocity falls below the electron's normal velocity in the atom. This is only an approximation to the actual case since no provision is made for electron pick-up; so one would not expect this approach to describe the behavior of the ion while passing through the final portion of the track even though it is capable of treating the total range of particles when their initial velocities are higher than in this difficult region. The study of the range-energy relation at low energies has been done experimentally.

The first attempts at doing this were made by Blackett[2] in 1923 by observing elastic collisions between alpha rays from radioactive substances and gas atoms in a cloud chamber. He observed 25 "air" atom recoils (N or O), 1 alpha, 9 argon ions, and 8 protons. If one measures the angles between the three tracks and the lengths of the tracks and estimates the energy of the alpha particles at the time of collision from its residual range, one can apply conservation of energy and momentum to find the energy of the recoil ion. By doing this for a number of collisions, a range-energy relation may be determined. The experiment was repeated in 1932 by Blackett and Lees[3], improving the statistics. They found curves for alpha particles, protons, nitrogen, oxygen, and argon ions. The same technique has been used by Eaton[4] for neon ions, Anthony[5] for sulphur ions, McCarthy[6] for neon ions and deuterons, and Wrenshall[7] for carbon ions.

This method has certain disadvantages. The straggling in the residual range of the alpha particle introduces an uncertainty in its energy even if one has a fairly accurate range-energy relation for the α

particles. As pointed out by Livingston and Bethe[8], Blackett and Lees' results should have the energies increased by about nine percent because of the inaccurate alpha range-energy relation available at that time. Straggling on the part of the recoil ion in question is, of course, an intrinsic feature of the range-energy relation and will introduce scatter into data taken by any technique. Another disadvantage is the long and laborious task of collecting the data. All of the above experimenters were obliged to photograph some 750,000 to 1,000,000 alpha tracks in order to collect about 50 tracks suitable for measurement to yield the desired data.

1.2 Present Technique. The method used in the work presented here is the same, in principle, as the above method with the alpha particle replaced by the neutron as a bombarding particle. This procedure eliminates at least one of the above disadvantages. Since the neutrons leave no tracks in the cloud chamber, a high flux may be used to produce a higher rate of recoil production in the gas. Neutrons of a known energy may be produced by bombarding lithium with protons. The lowest energy ion one can record is determined by the shortest identifiable and measurable track. The present work was done with a chamber operating at a very low pressure, thereby increasing the length of track for a particle of given energy. The details of the experimental procedure are given in Chapter Two.

The cloud chamber used operates at a pressure before the expansion of approximately 45 millimeters of mercury. The composition of the gas is roughly forty percent water vapor and sixty percent permanent gas

(oxygen, helium, or argon) before the expansion. Following the expansion, the gas is predominately water vapor. When the chamber is operated with oxygen or argon, the stopping power of the gas during the sensitive time is 7.6 percent that of NTP air. When it is operated with helium, the stopping power is 5.7 percent of NTP air. This chamber is described in detail in Part Two of this paper. Figures 1 through 3 are photographs made with this chamber. The photographs are full size.

1.3 The Range-Energy Relation. Figure 4 shows the range-energy relation as determined for protons in the chamber. The curve is based on 36 proton tracks collected during three separate runs with the chamber filled with oxygen and water vapor, and nine tracks collected in a run using argon and water vapor, a mixture which has almost the same stopping power. Four adjusted points are also included for runs using helium and water vapor.

Figure 5 shows the range-energy relation as determined for oxygen ions in the chamber. The curve is based on 38 oxygen tracks collected during three separate runs with the chamber filled with oxygen and water vapor, and seven tracks collected in a run using argon and water vapor. Eleven adjusted points are also included from runs using helium and water vapor.

Figure 6 shows the range-energy relation as determined for alpha particles. The curve is based on only 17 points collected during two runs with the chamber filled with helium and water vapor. The chamber did not work as well with helium, having a smaller sensitive region. It was not considered practical to spend a large amount of time to collect a greater number of tracks.

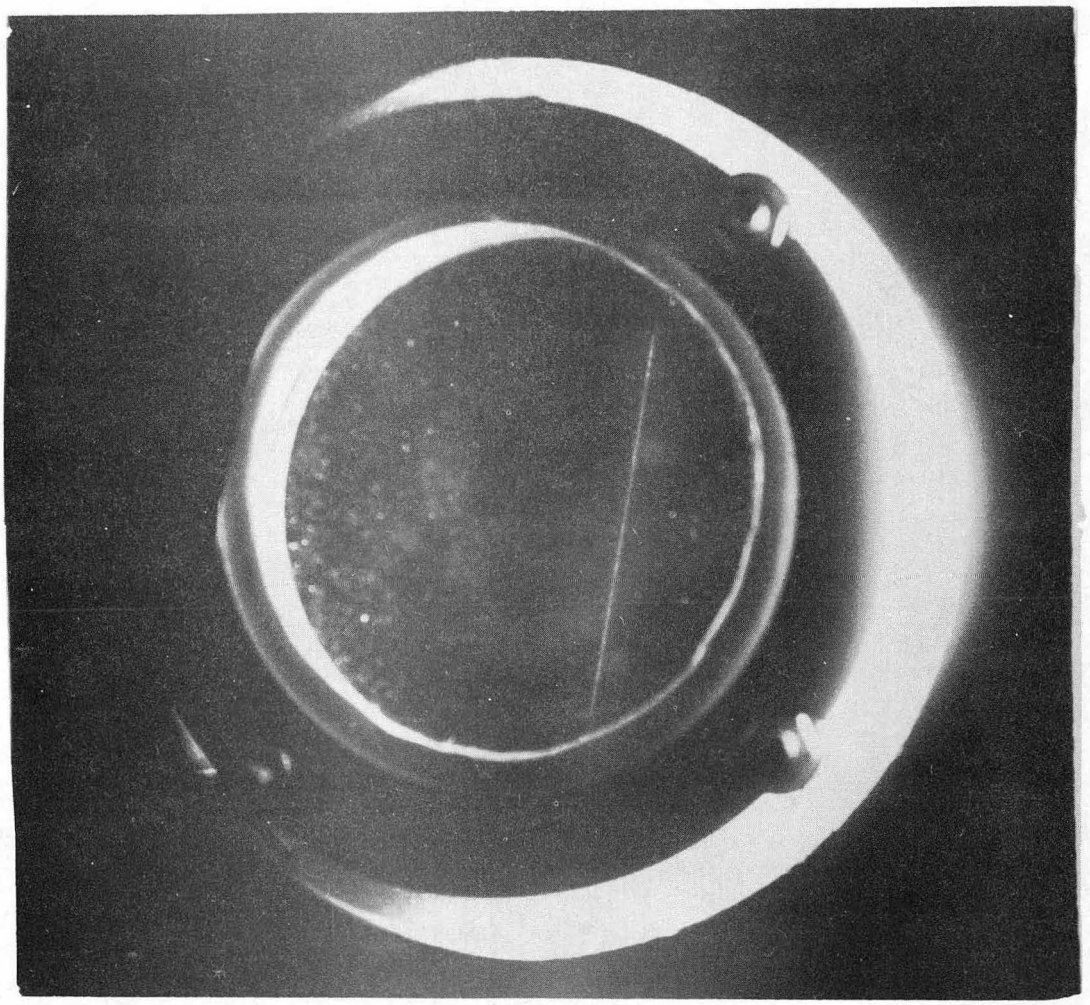

Fig. 1

A proton is struck by a neutron of 360 kev entering from the top of the picture. The proton recoils with an energy greater than 250 kev and passes out of the sensitive region. Many tracks had to be discarded for this reason. The photograph is full size.

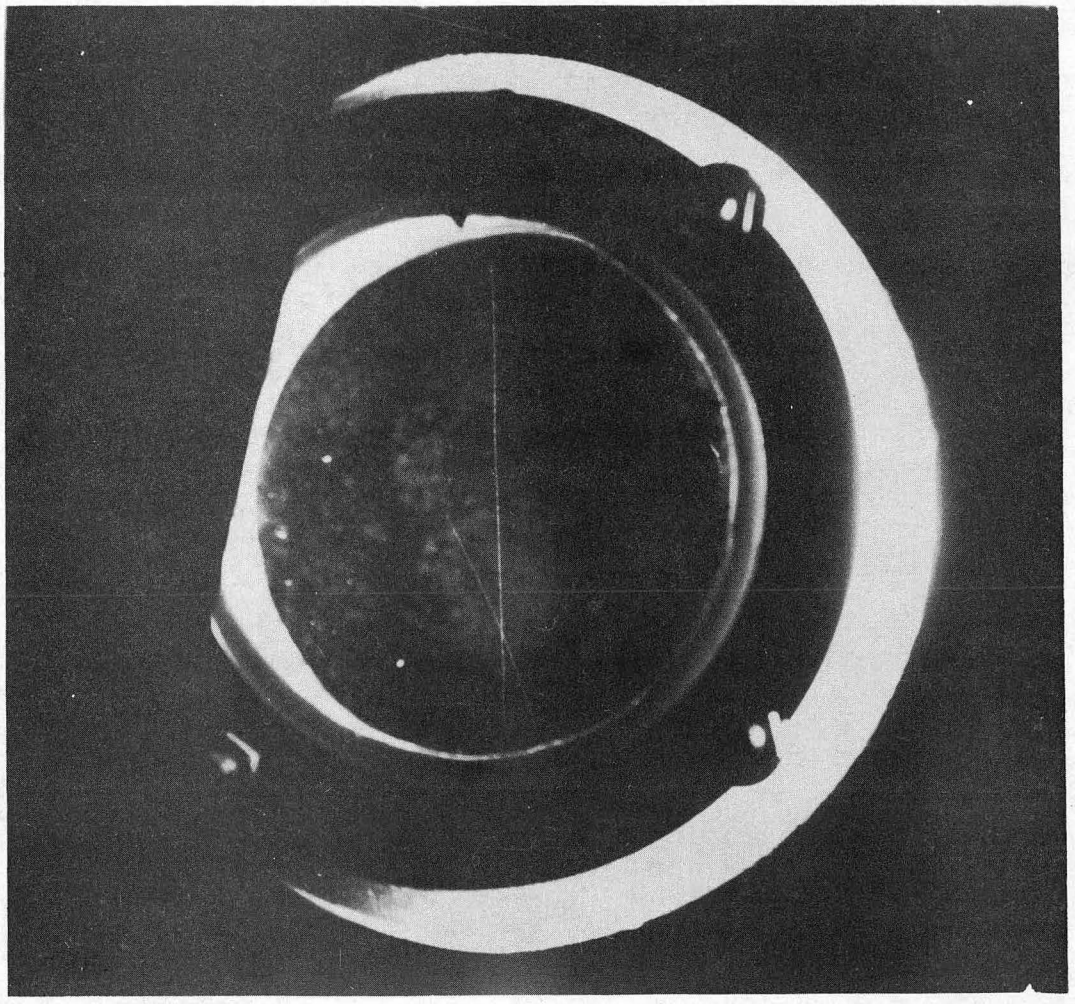

Fig. 2

A very unusual picture showing a complete 260 kev proton recoil starting and stopping just within the sensitive region. The second track is a proton recoil of 85 kev.

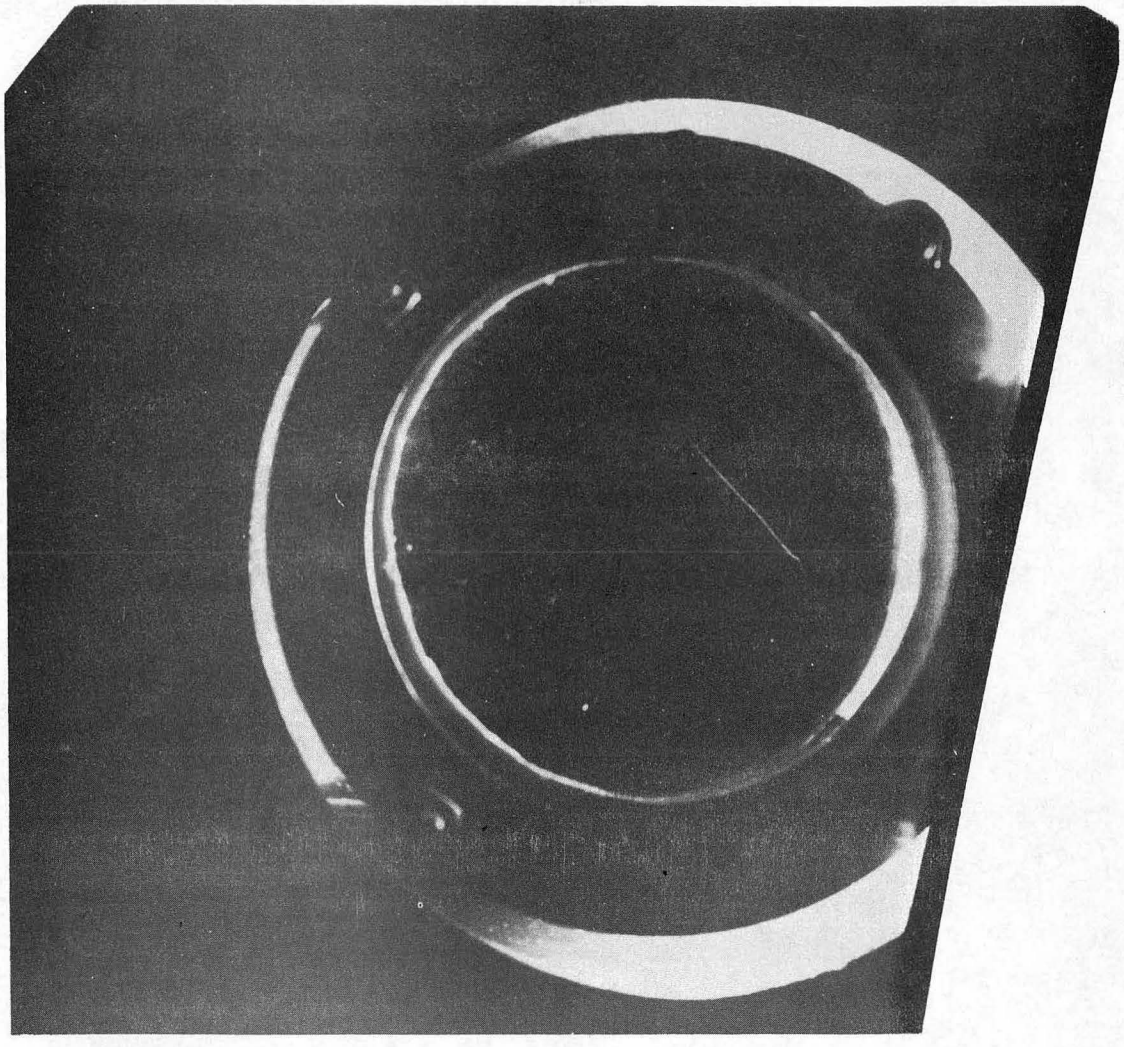

Fig. 3

A typical 160 kev proton recoil. This proton has been struck by a 265 kev neutron entering from the top of the picture. The photograph is full size.

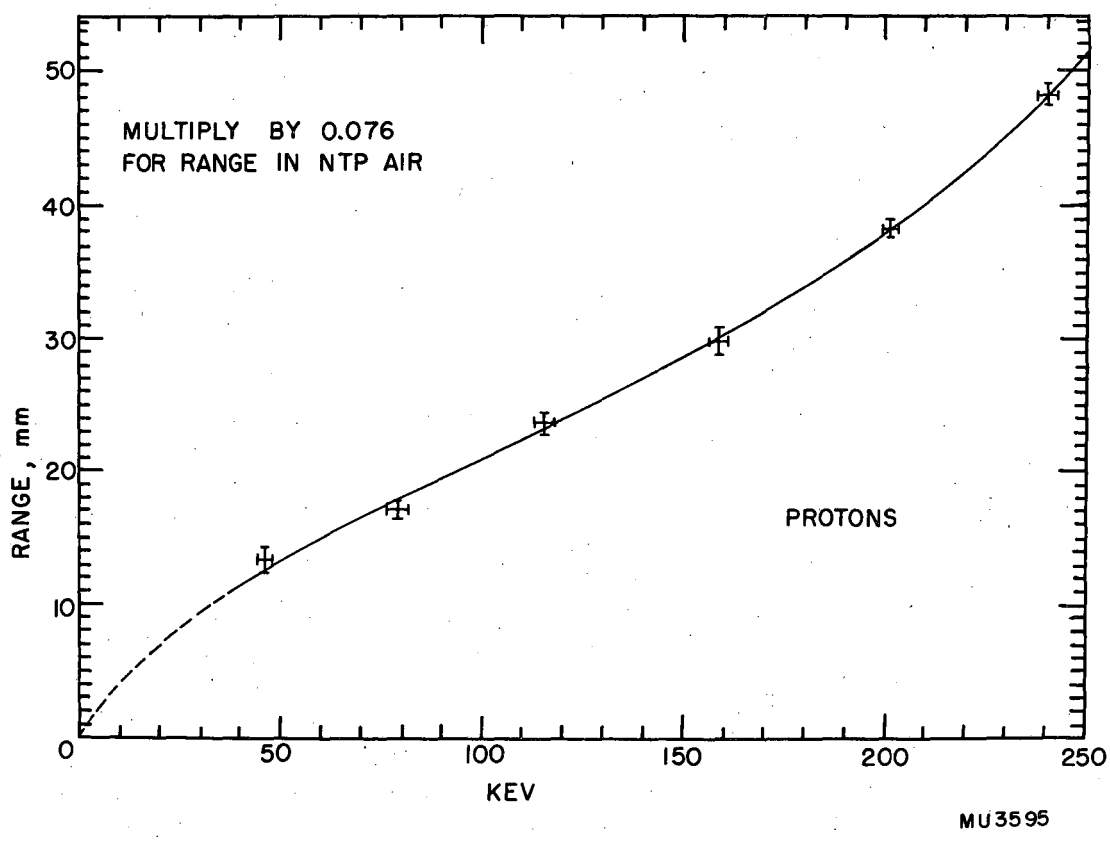
MULTIPLY BY 0.076
FOR RANGE IN NTP AIR
PROTONS
RANGE, mm
KEV
0
10
20
30
40
50
50
100
150
200
250
MU3595

Fig. 4

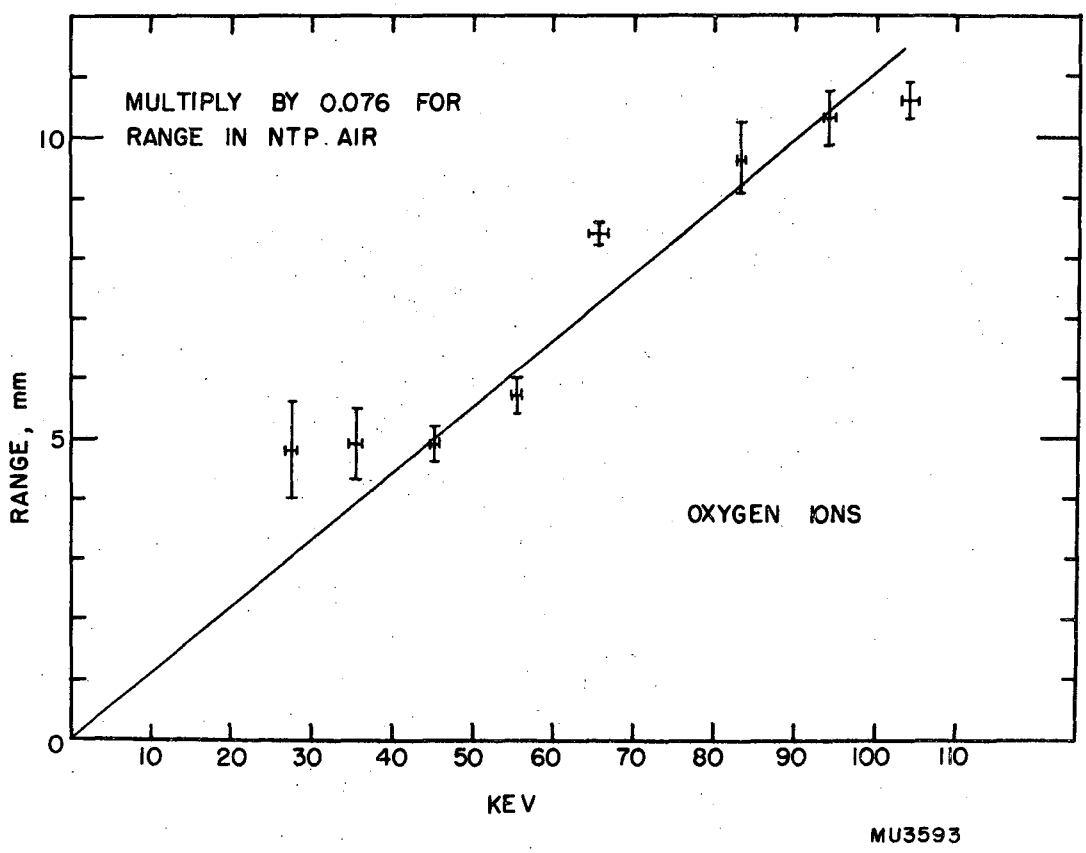
MULTIPLY BY 0.076 FOR
RANGE IN NTP. AIR
OXYGEN IONS
RANGE, mm
KEV
0
5
10
10
20
30
40
50
60
70
80
90
100
110
MU3593

Fig. 5

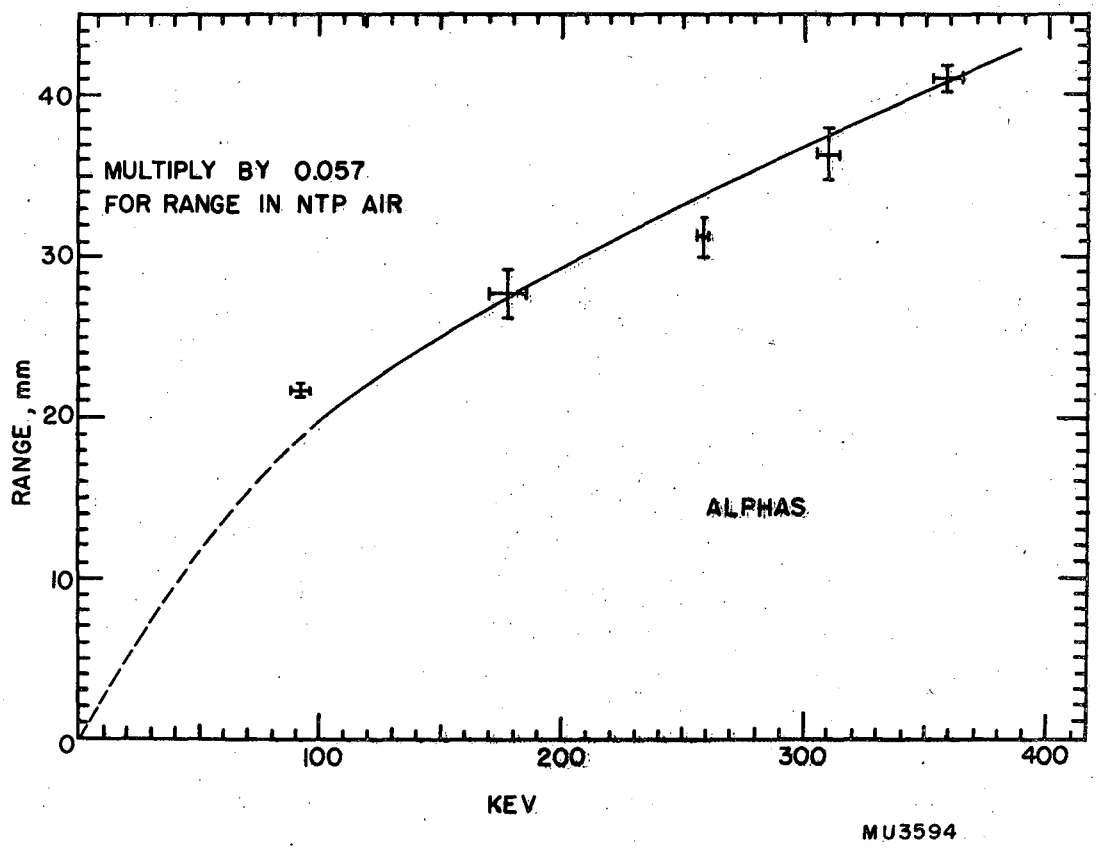
MULTIPLY BY 0.057
FOR RANGE IN NTP AIR
ALPHAS
RANGE, mm
KEV
0
10
20
30
40
100
200
300
400
MU3594

Fig. 6

Recently Bethe[9] has published best estimates of the range-energy relations for protons and alpha particles. His results, those of Blackett and Lees[3], corrected as suggested by Livingston and Bethe[8], and the results of this work are plotted together in Figure 15 of Chapter Three. The curves are seen to be in essential agreement.

Blackett and Lees' curve for alpha particles is based on 38 tracks ranging in energy from 34 to 1900 kev. Their proton curve is based on 69 tracks, of which 50 fall in the energy range covered by this work. Their oxygen data do not extend below 200 kilovolts, and they have only ten tracks of length between 1 and 2 mm.

Chapter Two

Experimental Procedure

2.1 Method. To measure the range-energy relation it is necessary to produce particles of known energy and then measure their path length. In this experiment the path length is measured by photographing the tracks in the cloud chamber with a stereoscopic camera and reprojecting the processed film through similar lenses to produce an image the same size as the original object. It may then be measured with a millimeter scale. The camera and projector used were the standard equipment of the UCRL cloud chamber group as developed by Powell and described by Brueckner et al.[10] except that auxiliary lenses of +1 diopter were attached to enable them to work closer to the small cloud chamber than the distance used for more conventional sized chambers.

The energy of the recoil ions can be determined by producing them with elastic collisions with monoenergetic neutrons. Lithium seven has a threshold for a (p,n) reaction of 1.882 Mev determined most accurately by Herb, Snowden, and Sala[11]. If one bombards lithium with protons of known energy, he will get neutrons of a definite energy at any particular angle of observation. The energies available are shown in Figure 11. In this experiment neutrons were used at 0° to the proton beam where the energy of the neutrons varies slowly with the angle.

In an elastic collision, the maximum energy transferred to the struck particle, E_o, is given in terms of the energy of the bombarding

particle, E_n, by

$$E_o = \frac{4\,Mm}{(M+m)^2}\ E_n \qquad (1)$$

where M and m are the masses of the two particles. This maximum transfer of energy is accomplished when the recoil particle is projected straight ahead. If the recoil is at an angle, θ, its energy, E, is given by

$$E = E_o \cos^2 \theta. \qquad (2)$$

If one can find the angle between the direction of the neutron and the direction of the recoil, the energy may be calculated. The direction of the invisible neutron path may be determined if one has an effective point source of neutrons, since the beginning of the recoil track determines the trajectory of the neutron before the collision.

2.2 Arrangement of Apparatus. Figure 7 is a plan view of the experimental arrangement. Protons are accelerated in the UCRL Van de Graaff generator to an energy which was changed from run to run, but which was always in the neighborhood of 2 Mev. The protons are turned through 90° by a magnet, passed through a collimator and strike the evaporated lithium film target, where neutrons are produced. The protons stop in the 10 mil tantalum cap supporting the lithium. The neutrons enter the cloud chamber ten inches away through 10 mil tantalum windows. The cloud chamber is mounted on a movable table which also carries the camera tube and all associated control electronics. See Figure 8. The particular filling gas to be used is supplied through a trap from a compressed gas cylinder. The camera rests on top of the camera tube looking into the chamber through the cover glass.

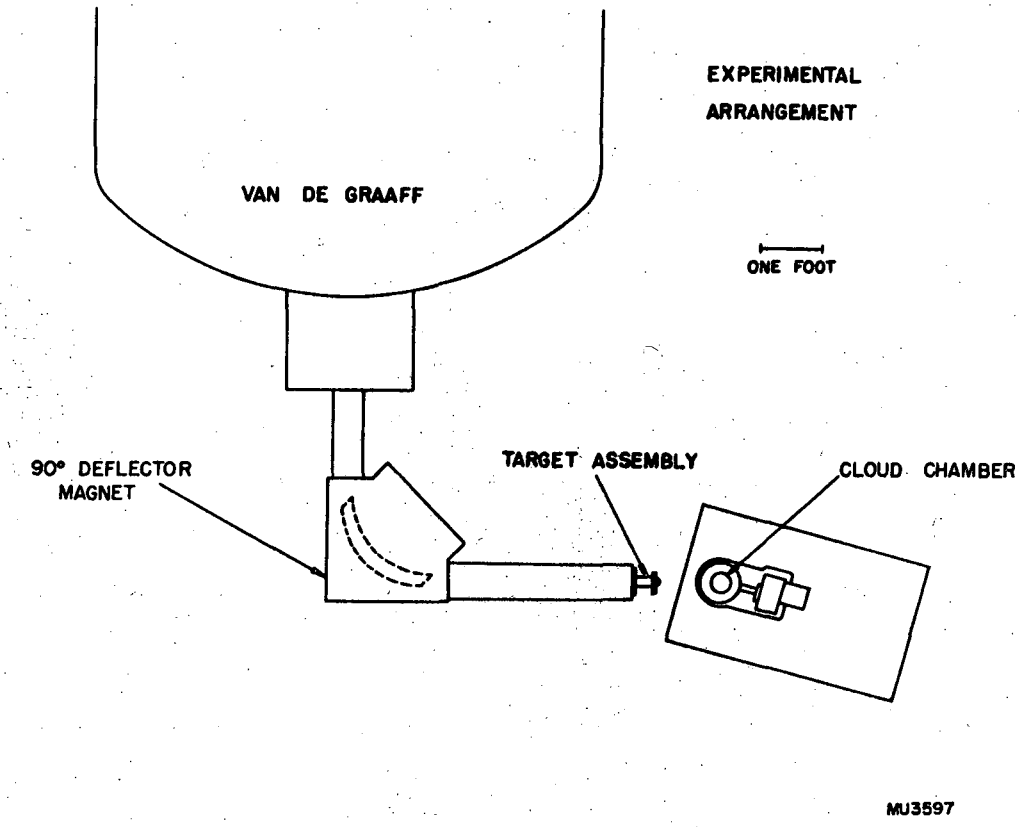
EXPERIMENTAL
ARRANGEMENT
VAN DE GRAAFF
ONE FOOT
90° DEFLECTOR
MAGNET
TARGET ASSEMBLY
CLOUD CHAMBER
MU3597

Fig. 7

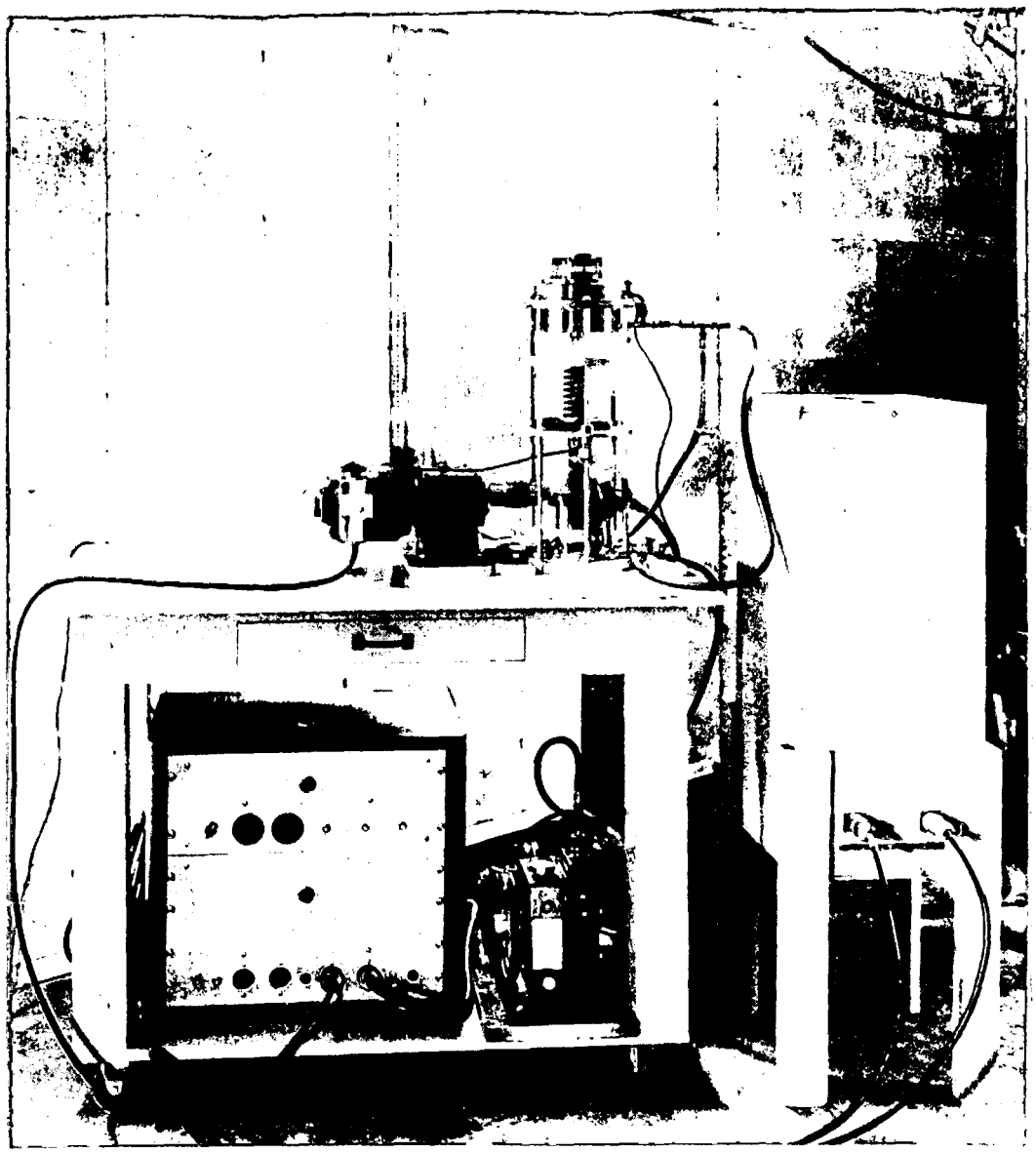

ZN282

Fig. 8

The table is carefully positioned in front of the target cap with the aid of a lining-up jig which attaches to the top of the chamber. The adjustment is made so that the window of the chamber is ten inches from the lithium film, and the direction of the proton beam bisects the chamber.

2.3 Target Assembly. Figure 9 shows the construction of the lithium target assembly. The main features are: 1) A carbon collimator of 1/4 inch diameter which defines the extent of the neutron source. 2) A carbon shutter which is actuated by an electromagnet. This catches the proton beam except when the shutter is raised for the two or three seconds in which the target is bombarded for one expansion of the chamber. 3) An insulated copper block electrically connected to an external terminal. When the shutter is closed, it contacts this block and the beam current may be monitored by a microammeter. The energy of the protons fluctuates continually and the Van de Graaff operator is able to maintain the beam at proper energy by observing the beam current at this point and controlling the belt spray current as needed. 4) The tantalum cap carrying an evaporated lithium film on the inner surface. The cap is domed outwards to get the neutron source as far forward of the brass mountings as possible to minimize the effect of scattered neutrons. The retaining ring is beveled for the same reason.

2.4 Method of Target Preparation. The lithium is deposited on the tantalum cap by evaporation in vacuum. The cap is supported a few inches above the lithium source behind a mask with a central circular opening of area 28.16 cm^2. The lithium source is a thin walled stainless steel crucible, 5/16 in. in diameter and 1-1/4 in. long, that is filled about three-

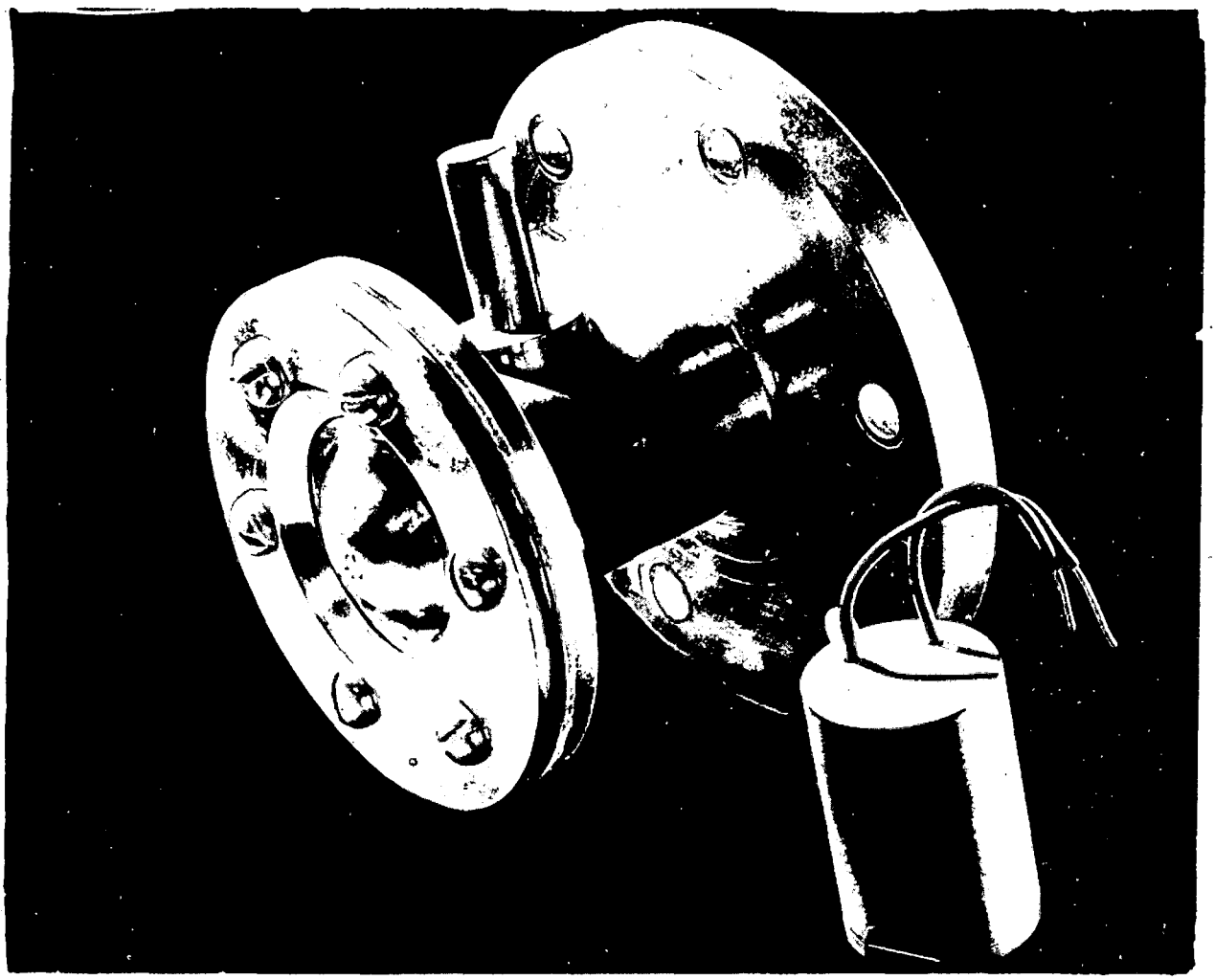

Fig. 9A

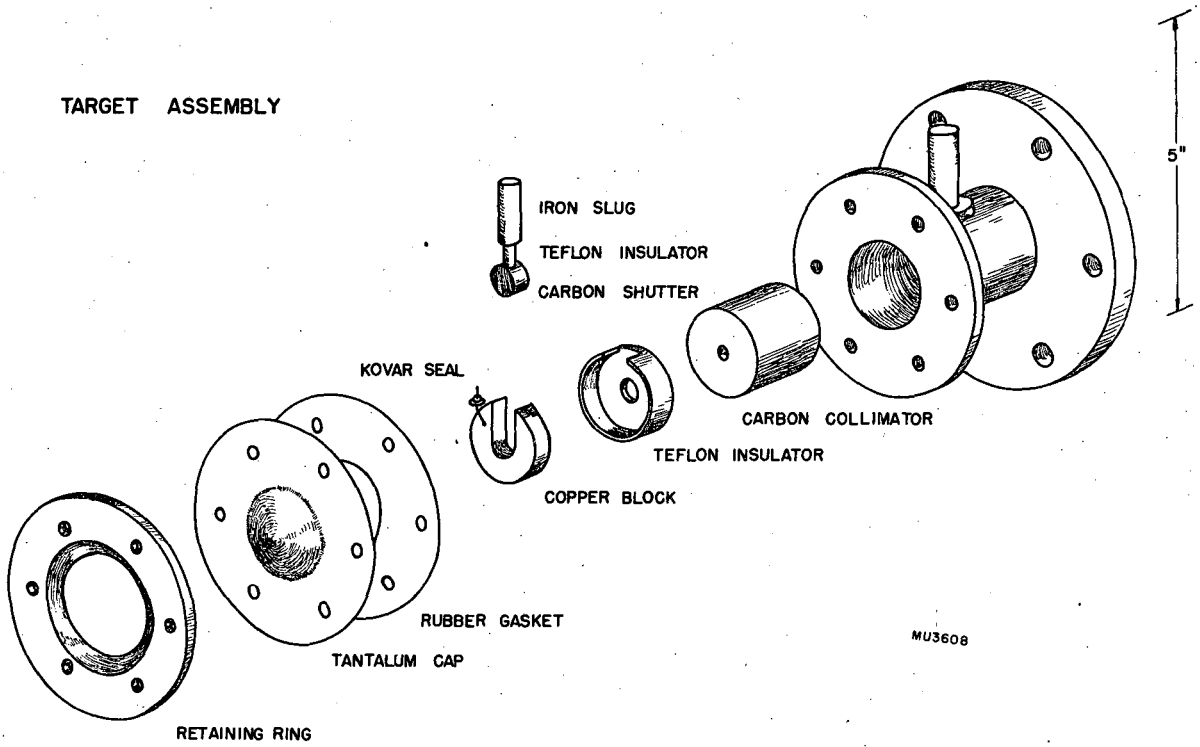
TARGET ASSEMBLY
IRON SLUG
TEFLON INSULATOR
CARBON SHUTTER
5"
KOVAR SEAL
CARBON COLLIMATOR
TEFLON INSULATOR
COPPER BLOCK
RUBBER GASKET
TANTALUM CAP
RETAINING RING
MU3608

Fig. 9

quarters full with small pieces of metallic lithium cut from a small block of the metal. The charged crucible is placed in a small quartz beaker (1/2 in. diameter by 1-1/4 in. long) which fits snugly in a coil of tungsten heater wire. The apparatus is placed under a bell jar and pumped to less than one micron pressure. It is very difficult to get consistent amounts of lithium deposited from one evaporation run to another. A procedure was finally adopted that gave results consistent to about ± 30 percent with an occasional target coming out twice normal weight for no obvious reason. The process begins on the second day before a target is needed for a run. The tantalum cap is thoroughly washed with soap and water and rinsed in distilled water followed by acetone. The crucible is charged with lithium and the assembly pumped down to low pressure (10 to 20 microns). The filament is then heated with about 150 watts input for about 30 seconds which drives the pressure up to 80 or 90 microns. After this is pumped out, the heating is repeated. The time of heating is gradually increased to a maximum of between two and two and a half minutes, while the adsorbed gases are driven off. By the end of several reheatings, occupying perhaps twenty minutes, the pressure should not rise above 10 microns on heating and should pump out rapidly to the order of one micron when the heater is turned off. The heater should not be operated for more than two and one-half minutes during the outgassing, or lithium will begin to evaporate. A small amount is usually carried over during the outgassing, but this causes no difficulty. After the outgassing period the apparatus is left under the diffusion pump overnight. The next morning the pressure

should be well under one micron and the evaporation may be made.

The tungsten heating coil is supplied with about 125 watts of power (14 amperes at 9 volts, the exact values of which do not seem to be critical), and the heating period is carried on for about eighteen or twenty minutes. After switching off the heater, one allows the apparatus to cool for several minutes before removing the target for weighing.

Lithium is extremely active chemically and certain precautions must be followed in handling it if one is to avoid oxidation and the resulting thickening of the target. When the lithium film first comes from the evaporator it has a clean, attractive, metallic appearance with a slight yellowish cast. Upon exposure to the air it rapidly darkens and soon becomes black. The tantalum caps used weigh thirty grams, while the total mass of lithium deposited on the exposed surface of an acceptable target was allowed to vary between nine and fifteen milligrams. This gives targets of thickness approximately 0.3 to 0.5 mg/cm^2. Figure 10 shows the mass of three targets as a function of time after exposure to air. The final masses after two days appear beside each curve. The weighings are done on a chain balance to one-tenth of a milligram. After two days the target has a satiny white appearance and is probably hydrated lithium hydroxide. It is the presence of a delay of about three minutes before rapid oxidation sets in that allows one to handle and weigh these targets without elaborate precautions. The clean targets become "dirty" very promptly after exposure to air and the very small target contamination which takes place during the first three minutes is plainly visible. The

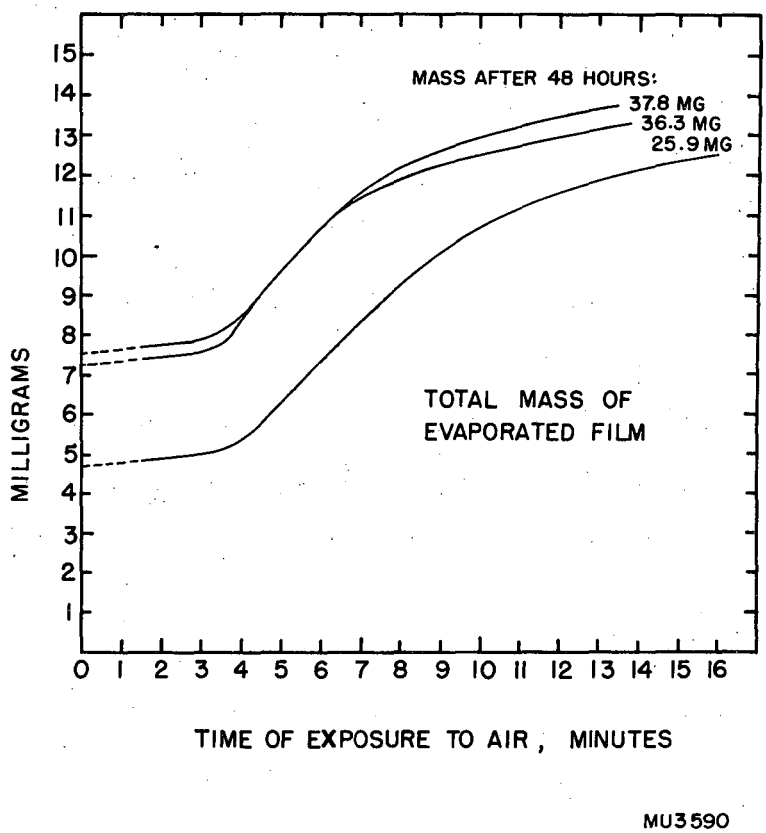
MASS AFTER 48 HOURS:
37.8 MG
36.3 MG
25.9 MG
TOTAL MASS OF
EVAPORATED FILM
MILLIGRAMS
TIME OF EXPOSURE TO AIR, MINUTES
MU3590

Fig. 10

entire surface becomes completely black considerably before the initial rapid oxidation is complete. This means that one can tell at a glance whether a target is still suitable for use since one that is slightly dirty but which still appears yellowish through the film actually is only slightly contaminated.

When the evaporated target is removed from the evaporator, it is promptly put into a vacuum desiccator which is then flushed and filled with argon. A clean tantalum cap is placed in the apparatus, the bell jar is quickly replaced and the evaporation system pumped down again before the lithium charge has time to oxidize. The chain balance is set to the midpoint of the acceptable mass range, which is usually within two or three milligrams of the correct value. After this adjustment, the finished target is transferred from the argon atmosphere to the balance, the final adjustment is made with the balance (which takes only a few seconds) and the target is returned to the argon atmosphere.

The first target is preserved in an argon atmosphere while a second is prepared. The evaporation apparatus is outgassed again, but this time only two or three heats of about 2 minutes each are required because of the very brief exposure to air. After this outgassing the evaporation is begun immediately. It is found that the second evaporation requires 2 or 3 minutes more running time than the first. The second target is handled in the same manner as the first, and the better one is selected for use. It is not advisable to attempt to prepare a third target from the same charge with the amount of lithium used in this apparatus

because the supply is near exhaustion and the third will frequently have very little deposit.

The prepared targets may be stored indefinitely in vacuum. To mount on the Van de Graaff, the target to be used is placed in a vacuum desiccator filled with argon and carried to the accelerator. The target assembly (Figure 9) is in place. The retaining ring, tantalum cap, and rubber gasket are removed, and the old cap set aside. The new one is placed in position with the retaining ring and gasket and placed on the end of the target assembly and pumping is begun immediately. Atmospheric pressure holds the cap tight while the machine screws holding the ring in place are tightened. By using this procedure it is possible to get a weighed and selected lithium target into working position on the Van de Graaff with less than two minutes total exposure to air and substantially no contamination.

2.5 Photography. Photography is done with Wollensak 127 mm Velostigmat lenses fitted with +1 diopter auxiliary lenses and opened to full aperture of f/4.5. The lenses are located 22 inches from the center of the cloud chamber. Illumination is provided by an FT-231 flash tube mounted behind a cylindrical Lucite lens placed 1-1/2 inches from the chamber wall. The flash tube is mounted inside the camera tube which surrounds the chamber when in operation. The tube is flashed from a 64 microfarad capacitor charged to 2400 volts. This voltage is a little higher than that recommended for the tube, but it was desired to get full light energy without going to a larger condenser bank. The tube has operated satisfac-

torily for several months. Exposure is made on Eastman Linagraph Ortho film which is developed for 14 minutes in D-19 developer at 20° C.

2.6 Sequence of Operations. The first few runs were begun by calibration of the Van de Graaff voltage in terms of the threshold for the $Li^7(p,n)Be^7$ reaction at 1.88 Mev. A BF_3 proportional counter, surrounded by a one inch paraffin wall, was placed on the axis of the proton beam-lithium target system and two or three feet beyond the target. The 90° deflector magnet has been provided with an electronic current regulator which automatically maintains the magnet current at any value for which it is initially set. The current can be set reproducibly to an accuracy of about 1/2 percent to currents in the neighborhood of one ampere. At currents of 0.98 amperes no neutrons were counted except background, while at a current of 0.99 amperes neutrons were counted at a rate eight or ten times background. The magnet current which deflected protons of energy 1.88 Mev was taken to be 0.985 amperes to an accuracy of ± 1/2 percent. Since several subsequent repetitions of the calibration all gave the same result, the calibration procedure was eliminated in the last few runs. With one point of the energy-magnet current calibration established, the slope of the current-energy characteristics of a previous calibration was adopted for use in extrapolation. This procedure was justified by finding the 2.30 Mev peak in the neutron yield for Li^7 at the proper point. The calibration was found to be

$$E = 4.18\ I - 2.24,$$

where E is in Mev and I is in amperes. This expression is valid in the

range of energies between 1.5 and 2.5 Mev. Outside of this region the linearity of the magnetization curve cannot be depended upon.

After calibration of the Van de Graaff, the magnet current is adjusted to pass protons of the required energy as read from the graph given in Figure 11. The calculated points for Figure 11 are tabulated in Appendix I accurate to 10 volts neutron energy. The beam is steered and focussed to give maximum current into the shutter, and the belt spray control is adjusted by the operator to keep the beam coming into the shutter at all times. Optimum conditions yield about three microamperes average current of protons consisting of fifteen pulses per second, each one 400 microseconds long. This is a peak current of 500 microamperes and represents about 10^{12} protons per pulse. Using the differential cross section as given by Taschek and Hemmendinger[12] and the geometry of the experimental arrangement, one calculates an expected flux of 5×10^{4} neutrons per pulse through the chamber. With the chamber filled with oxygen and water vapor, this should yield about four recoils per picture, half of them protons, the other half oxygen ions.

The length of time between pulses is 67 milliseconds, while the sensitive time of the chamber is about 10 milliseconds, therefore it is necessary to control the timing of the proton pulse to coincide with the sensitive time of the chamber. This is done by inserting an extra pulse at the proper time into the stream of regular equally spaced pulses. The timing sequence is controlled by the cloud chamber. A microswitch is operated when the piston begins its descent, and this triggers the timing

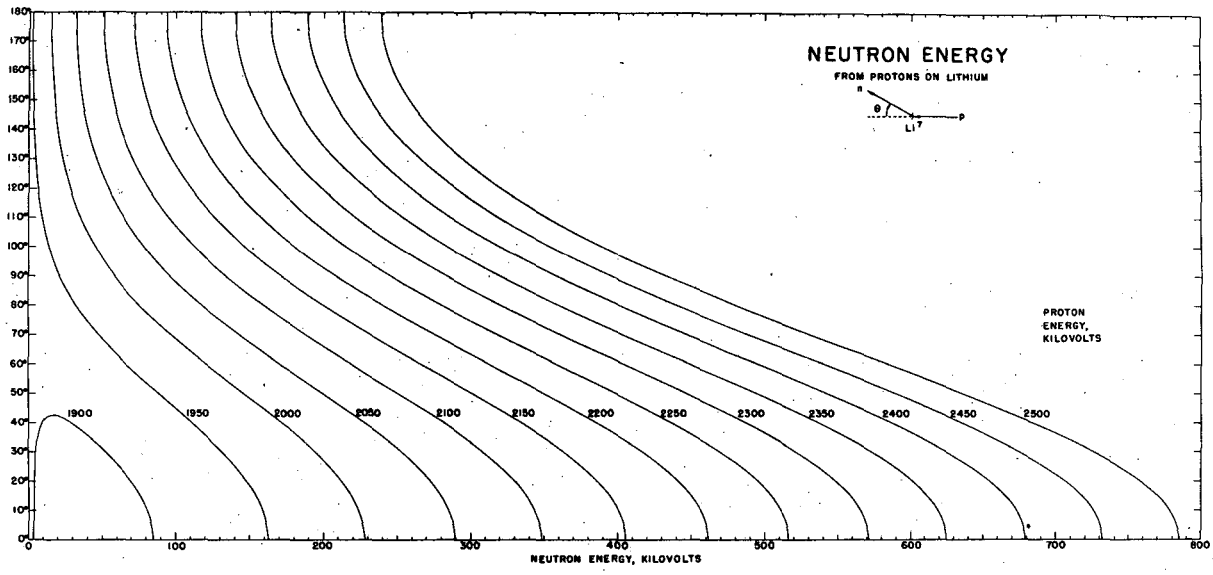
NEUTRON ENERGY
FROM PROTONS ON LITHIUM
n
θ
Li⁷
p
PROTON ENERGY, KILOVOLTS
1900
1950
2000
2050
2100
2150
2200
2250
2300
2350
2400
2450
2500
0
10
20
30
40
50
60
70
80
90
100
110
120
130
140
150
160
170
180
0
100
200
300
400
500
600
700
800
NEUTRON ENERGY, KILOVOLTS

Fig. 11

circuits. Call this time zero. At zero plus about 3 milliseconds the piston hits bottom, at zero plus 19 milliseconds the proton beam is pulsed, and at zero plus 30 milliseconds the light is flashed to take the picture. The optimum light flash delay was determined by placing an alpha source in the chamber and observing the photographs taken at various settings of the flash delay. The optimum proton pulse delay setting was determined by visually observing the number of recoils produced in the chamber and adjusting the proton pulse delay for maximum yield.

Photographs are taken at the rate of one a minute. At the end of a series of 10 or 15 pictures, the chamber is flushed with its filling gas and the pressure reset. This insures that any small leak present will not change the gas composition or increase the pressure to a value higher than the proper operating region. A normal run covered a period of eight hours, of which four hours or less were available for collecting data, during which between 100-150 exposures could be made. During the whole series of runs approximately 850 exposures were made which yielded a total of 122 suitable points for the various range-energy relations. This low yield rate is due to the following factors:

1) Failure of flash tube to fire. This occured in approximately 15 percent of the exposures.
2) Weak or missing proton beam at time of exposure. This occured in approximately 10 percent of the exposures.
3) Chamber not sensitive. A small leak in the chamber may raise the pressure above the operating region; or the

pressure may be initially set below minimum operating value. This occured in about 10 percent of the exposures.

4) Failure of electronics to insert an extra pulse at proper time. (Not proved but suspected since more pictures are blank than attributable to case 3 or statistical fluctuations.) Perhaps 10 percent.

5) Tracks visible, but leave sensitive region or illuminated region. Out of 800 tracks observed, only 170 were suitable for measurement.

6) Background. About 25 percent of the tracks measured were due to background. The background, consisting of recoil tracks scattered at random on the range-energy plot are presumed to be caused largely by scattered neutrons. Some are tracks which have left the sensitive or illuminated region without having been identified as such, and a few may be produced by the neutron background produced by the 30 or more microamperes of protons which strike the internal parts of the deflector magnet.

Number 5 is by far the most important reason of low track yield. Of these reasons for low yield, all but number two could probably be improved by further development of the chamber. See Chapter 4. The yield could also be almost doubled by increasing the lithium film thickness without excessive proton energy straggling being produced, although one should avoid introducing errors unnecessarily.

Chapter Three

Reduction and Interpretation of Data

3.1 Measurements and Calculations. The processed film is projected to form a full size space image. A movable stand is positioned by measurement so that a point on it is in the proper location to represent the neutron source. A string is attached to this point to be used to represent the neutron path. A translucent projection screen, called the space table, is mounted so that the screen may be rotated and tipped around two mutually perpendicular axes into any possible plane and the two angles measured by means of attached graduated scales. The space table is adjusted so that its central reference line passes through the initial point of the track to be measured and its direction passes through the simulated neutron source. The string attached to this point is used as an aid in this adjustment. The entire projection system is diagrammed in reference eight. The dip and azimuth angles, α_1 and β_1 for the neutron path can now be read from the graduations on the space table. The space table is readjusted to contain the track itself, and the dip and azimuth angles, α_2 and β_2, of the track are recorded and the length of the track measured. The length measured was the total path length traversed by the ionized particle. The space relations of the four angles measured to the desired angle, θ, are shown in Figure 12, together with the proper formula for computation. Because the height of the illuminated region of the cloud chamber is small (~3/4 inch), and the neutron source is almost a foot

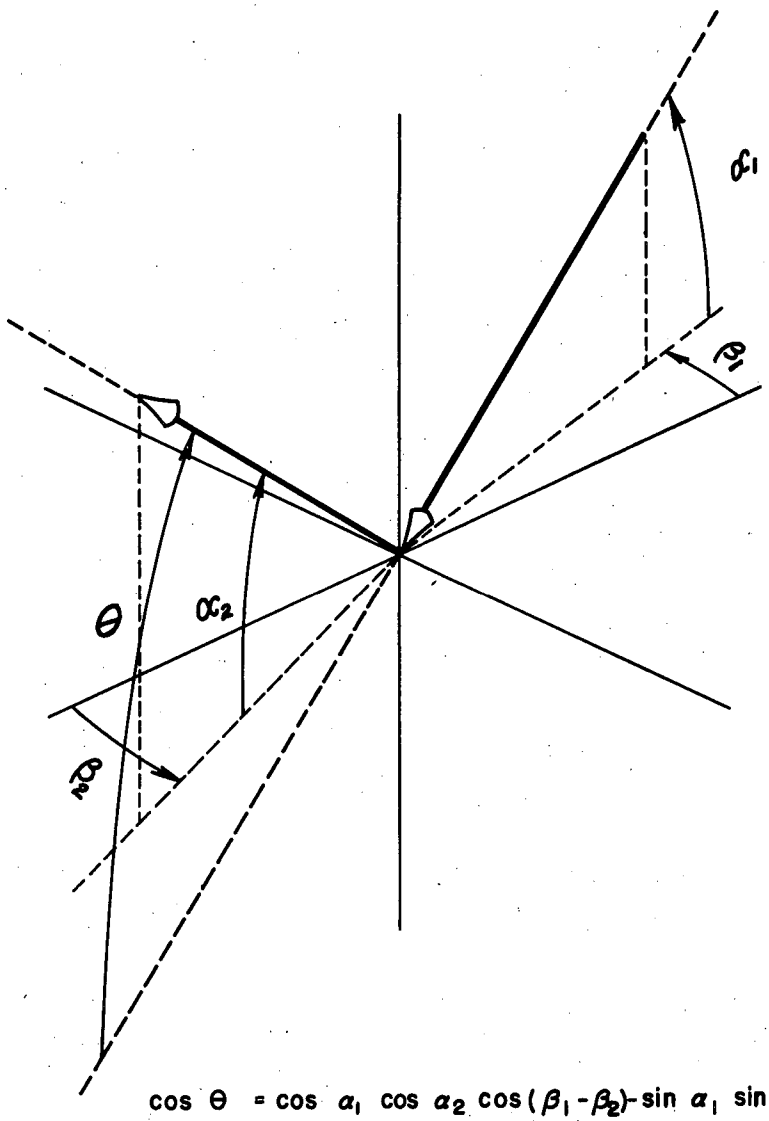

$$\cos\Theta = \cos\alpha_1 \cos\alpha_2 \cos(\beta_1 - \beta_2) - \sin\alpha_1 \sin\alpha_2$$

MU3586

193

Fig. 12

away from the center of the chamber, α_1 is almost always within 2° of the horizontal. Consequently the second term may be neglected in many cases, and the calculation can be done very quickly by multiplying with the S scale of a slide rule.

Knowing the energy of the proton beam by means of the calibrating procedure described in section 2.6, one can determine the neutron energy in the forward direction from Figure 11, and determine the maximum recoil energy for the various kinds of atoms present in the gas of the cloud chamber by using equation (1). The measurement of θ, described on page 32, permits calculation of the recoil energy using equation (2). This computation was facilitated by constructing the nomograph shown in Figure 13. The numerical data for the construction of this nomograph constitute Appendix II. This has been calculated accurately to enable a large scale presentation of all or part of the chart if needed. An alignment chart may be linearly magnified in any direction and the scales may be slid with respect to one another if two are moved proportionally. It is worthwhile constructing such a chart if a large number of the same type of calculation is to be done. The original of the nomograph, 18 inches by 30 inches, is accurate to 0.1 percent.

Most runs were made with oxygen and water vapor filling the chamber so that there were only two kinds of atoms in the gas. When the data are plotted, the points are seen to fall into two distinct groups. This makes possible the identification of the recoils. This procedure is satisfactory for particles whose masses have large ratios, but it

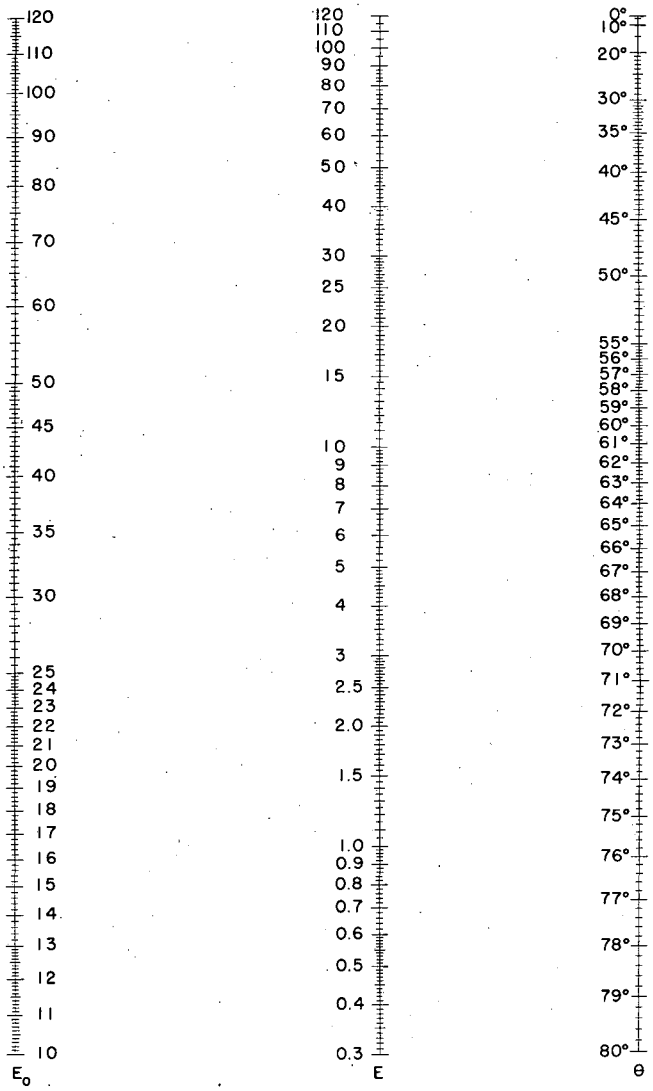
120
110
100
90
80
70
60
50
45
40
35
30
25
24
23
22
21
20
19
18
17
16
15
14
13
12
11
10
E_0
120
110
100
90
80
70
60
50
40
30
25
20
15
10
9
8
7
6
5
4
3
2.5
2.0
1.5
1.0
0.9
0.8
0.7
0.6
0.5
0.4
0.3
E
0°
10°
20°
30°
35°
40°
45°
50°
55°
56°
57°
58°
59°
60°
61°
62°
63°
64°
65°
66°
67°
68°
69°
70°
71°
72°
73°
74°
75°
76°
77°
78°
79°
80°
θ
$E = E_0 \cos^2 \theta$
MU 3528

Fig. 13

would be difficult, if possible at all, to distinguish, say, nitrogen from oxygen recoils. In recording the points on a graph while measuring the data, one can use different energy scale factors for each species of particle, with the unit energy interval chosen inversely proportional to the factor $4\ mM/(M + m)^2$, and record all curves on the same sheet. If this is done, an identification error will not misplace a point; so one can call each track by any name he pleases, and the resulting data will cluster automatically into the proper particle groups. The clustering of points in the same region for different runs with entirely different neutron energies provides evidence that a true range-energy relation and not a spurious background effect is being measured. Figure 14 presents all the raw data taken with water and oxygen filling, illustrating the results of this procedure.

3.2 Treatment of Data. Three plots similar to Figure 14 were made altogether, one for data taken in water vapor and oxygen (as shown), one for water vapor and argon, and the third for water vapor and helium. The data from the oxygen and argon runs were combined directly since argon and oxygen have very similar stopping powers and these gasses constitute only about 25-35 percent of the total during the sensitive time of the chamber. Furthermore, the clustering of the proton and oxygen points from the runs using these gasses fell on top of one another. The proton data were divided into groups falling in the ranges: 20-60, 60-100, 100-140, 140-180, 180-220, 220-240 kev. In each group the energy and range of each track was listed and the average of each taken for the group.

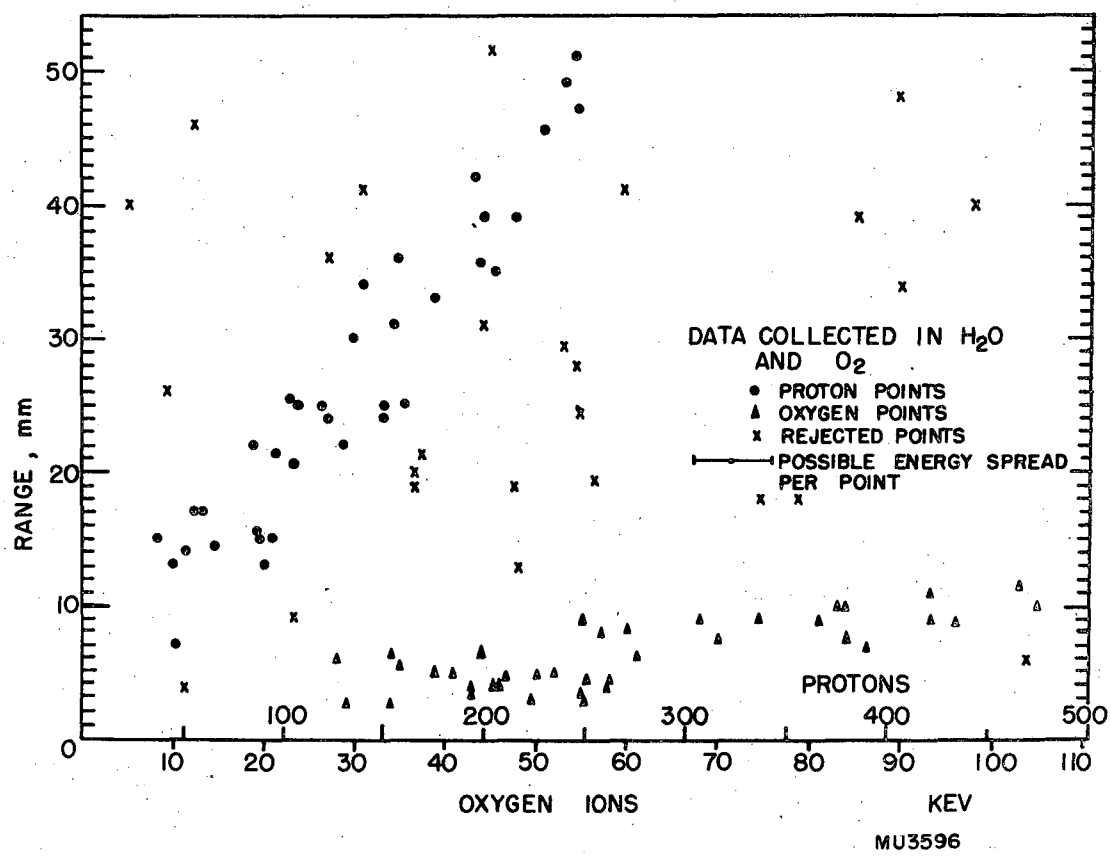
RANGE, mm
0
10
20
30
40
50
DATA COLLECTED IN H_2O AND O_2
PROTON POINTS
OXYGEN POINTS
REJECTED POINTS
POSSIBLE ENERGY SPREAD PER POINT
PROTONS
100
200
300
400
500
10
20
30
40
50
60
70
80
90
100
110
OXYGEN IONS
KEV
MU3596

Fig. 14

The probable error assigned for each is the probable error of the mean as calculated from the residuals. The oxygen data were treated similarly with intervals of ten kilovolts rather than forty. A similar treatment was applied to the alpha particle data taken in helium. The first use made of these preliminary results was to calibrate the approximate stopping power of the gas in the chamber relative to NTP air. The curves recently published by Bethe[9] and the curves of Blackett and Lees[3] with energy increased by 9 percent as recommended by Livingston and Bethe[8] were adopted as guides. Ratios of track lengths for the points determined in this experiment were taken to the lengths for corresponding energies according to the earlier curves, and rough averages were taken to determine the tentative relative stopping power of the cloud chamber. This procedure is founded on the assumption that the stopping power of the gas is independent of the energy of the particle, and this must be justified since it is not true for all gasses.

This question has been investigated by Crenshaw[13] who has published the stopping power relative to air of water vapor, deuterium, hydrogen, and helium in the energy range of 60 to 360 kilovolts incident proton energy. His curves show helium and water vapor to be essentially constant in relative stopping power throughout this region. The water vapor curve may be down by about five percent near the top, although this may not be significant. Data of Aron et al.[14] indicate that in the 1 Mev region the relative stopping power is the same as the value between 100 and 200 kev. Therefore, until this question has been inves-

tigated in more detail, it would seem satisfactory to assume constant stopping power for water vapor and helium, relative to air in this energy region. The behavior of oxygen is essentially the same as that of air.

An independent check permits final adjustment for best values of the relative stopping powers. The above procedure gives tentative values of relative stopping power of the water vapor-oxygen mixture (from the proton curve) and of the water vapor-helium mixture (from the alpha curve) with respect to air. A check on these is provided from the fact that oxygen tracks occur in both, and from these one can find the relative stopping power of the two different mixtures used in the cloud chamber. This number should equal the ratio of the two tentative values of relative stopping power for water vapor-oxygen and water vapor-helium mixtures. The three ratios so found were adjusted for consistency, the changes being small and not great enough to carry them out of their predicted ranges.

Having determined the best estimate of the relative stopping power of the water vapor-helium mixture to the water vapor-oxygen mixture, one can apply this factor to reduce the ranges of proton and oxygen ion tracks found in the helium runs to equivalent range in the oxygen runs. All the data are then collected, placed in groups as described above, and the final points for the range-energy relations calculated. The final results are plotted in Figures 4, 5, and 6 in Chapter One. The ranges, reduced to NTP air, are shown in Figure 15 in comparison with the results of Blackett and Lees[3] and the weighted curves of Bethe[9]. The relative value of ranges of protons, alpha particles, and oxygen ions as found in

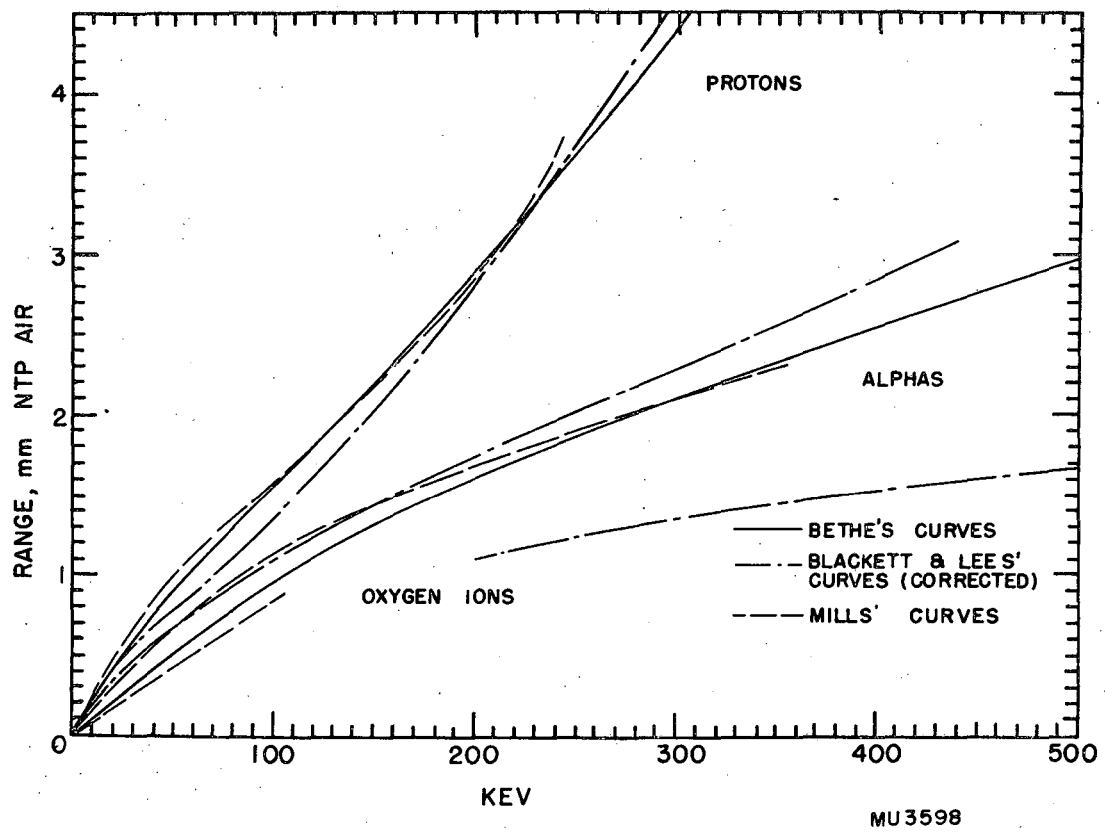
PROTONS
ALPHAS
OXYGEN IONS
BETHE'S CURVES
BLACKETT & LEE'S CURVES (CORRECTED)
MILLS' CURVES
RANGE, mm NTP AIR
KEV
0
1
2
3
4
100
200
300
400
500
MU3598

Fig. 15

the present experiment should be reliable to about seven percent, but the reduced ranges for NTP air are probably accurate to only ten percent.

3.3 Errors. In order to determine a point on the range-energy relation from observation on a track, it is necessary to determine the following quantities: the energy of the proton producing the reaction and, in turn, the energy of the neutron, the scattering angle, Θ, between the path of the recoil and the path of the neutron, and the track length of the recoil. In addition to the error introduced in determining these quantities, there is the possibility of a variation in the conditions under which measurements are made. This would occur if the stopping power of the gas in the chamber were not a constant due to either re-evaporation, operation at different initial densities, or temperature effects. Range straggling is another source of scatter in the data.

The greatest source of error is the uncertainty in the proton energy. The proton energy is controlled by the 90° deflection magnet of fifteen inch radius and the exit collimator of one-quarter inch diameter located immediately in front of the target. The uncertainty in the value of the energy of a proton derives from the uncertainties in the magnetic field and in the radius of curvature of the path of the proton. The percent uncertainty in energy introduced by the field control is twice the percent uncertainty in the field, and the percent uncertainty introduced by the finite exit slit width is twice the percent uncertainty in the radius. This gives a maximum error of one percent due to the field and of one and two-thirds percent due to collimation. Assuming the probable

error in each case to be one-half the maximum, one arrives at a one percent probable error in the proton energy, or 2000 ± 20 kev. This uncertainty in the proton energy produces approximately the same uncertainty in the neutron energy. This error is shown in Figure 14, and is seen to be sufficient to account for the scatter of the points. Other possible causes of variations in the neutron energy are proton energy straggling in the target, and variations in the angle of production of the neutrons. No effects of straggling were ever observed during the Van de Graaff energy calibration runs. The diameter of the chamber and its distance from the neutron source allows a maximum variation of neutron angle around 0° of $\pm 5^{\circ}$. Reference to Figure 11 shows that this variation introduces a negligible uncertainty in the neutron energy.

Consideration of the possible proton paths and the accuracy of the reprojection apparatus give the probable error of the scattering angle determination to be about two degrees. The energy of the recoil is given by equation (2), and the relative uncertainty of the energy is given by $|dE/E| = 2 \tan \theta \, d\theta$. This is unimportant at small angles, but becomes important at large angles where the recoil energy becomes small. No tracks were accepted at very large angles ($>70^{\circ}$), and since the absolute uncertainty in the neutron energy due to the uncertainty in the proton energy is small at these angles, this effect dominates the error of the lowest energy recoils. Even so, the absolute uncertainty of the energy of the recoils at low energies is in general less than those at higher energies, typical values being in the range of 15 kev in the case

of protons. The decreasing effect of the proton energy uncertainty as one goes to lower recoil energies combines with the increasing effect of the angle uncertainty to keep the absolute energy uncertainty fairly constant throughout the entire range of values.

Errors in the measurement of recoil length are negligible compared to the scatter of the data since the tracks can be measured to within a half millimeter with an ordinary millimeter scale. No effect has ever been observed attributable to a variation in the stopping power of the chamber. Data taken near the beginning and end of a run and from different runs fall on top of previous data. Straggling should produce less than 3 percent range error, since gas ion formation is a statistical process, and the lowest energy particles observed (30 kev) must make some 1000 ion pairs before coming to rest.

PART TWO: CONSTRUCTION AND OPERATION OF LOW PRESSURE CLOUD CHAMBERS

Chapter Four

Cloud Chamber Development

4.1 Previous Work. A cloud chamber operable at very low pressures has been described by Joliot[15]. His apparatus consists of a double piston arrangement, one being the piston of a volume controlled chamber, and the other, directly connected to it, acting as the piston in a linear pneumatic motor. The volume around the motor piston is evacuated prior to an expansion. To cause an expansion a special, wide-aperture valve is suddenly opened, admitting atmospheric pressure to the top of the piston. This sudden application of force to the motor piston produces a rapid expansion of the cloud chamber. Joliot was able to operate this chamber at very low pressures, reporting operation with pure water vapor and final pressure of thirteen millimeters. He finds very large expansion ratios, of the order of two (i.e. doubling the chamber volume), are necessary. The sensitive time of his chamber falls rapidly as the pressure is reduced, becoming only two milliseconds at the lowest pressures, and not rising to three milliseconds until the initial pressure is raised to 200 millimeters.

The present developmental program was begun with some tests on an existing small chamber similar in basic features to that designed by Joliot except that the piston was driven by compressed air and backed by atmosphere rather than driven by atmospheric pressure and backed by vacuum.

This chamber was mounted and modified to allow operation at reduced pressures, and tests on it seemed to show that it would be necessary to provide a large volume air reservoir of very high pressure if it were to ever operate at low pressures. An investigation of its possibilities was underway when it was destroyed in the fire that consumed Building 8 in the spring of 1950.

Since a fresh start was necessary, it was decided to completely change the basic design in an attempt to improve the chamber's performance. The experience with the first chamber and the report of Joliot's work indicated that the expansions were not fast enough. It was clear that the time of expansion in both cases was considerably longer than the sensitive time, and it was hoped that an increase in the speed of the piston descent would increase the sensitive time and reduce the necessary expansion ratio.

4.2 Chamber Design. The basic requirement governing the design of the cloud chamber was the need for a short expansion time of the order of the shortest sensitive time reported by Joliot[15], i.e., a piston descent time in the range of two to four milliseconds. This fast an expansion requires large driving forces of the order of 1000 pounds or more. A pneumatic arrangement to provide this would require either large piston areas or high driving pressures and in either case extremely large aperture valves to allow passage of relatively large amounts of air in a millisecond. Such arrangements were rejected in favor of a spring-driven linear motor as a more practical and compact mechanism. A standard industrial knock-out spring was selected for the linear driver which develops a force of

1200 pounds when compressed. Its spring constant is 120 pounds per 1/8 inch of compression, and it has a travel of 1-1/4 inches. This restricted travel means that the piston must be of larger diameter than that of the useful volume of the chamber if its motion is to double the volume. The chamber is compressed by a cam. The cam is turned at 4 R.P.M. by a Boston Ratiomotor of 1/12 H.P. capable of 360 inch-pounds of torque. A slow expansion from compressed position is made by reversing the motor, while a fast expansion is made by dropping off the edge of the cam. Large torques on the gear box at the moment of drop-off are avoided by a driving pin arrangement allowing the cam to shift 13° suddenly as soon as the piston develops a tangential force on the cam when it begins descent. Figure 16 is an assembly drawing of the chamber. The driving spring is not shown on this drawing. It fits between the spring thrust plate, part 28, and the guide support plate, part 8. The expansion ratio of the chamber is controlled by adjusting the position of the stop plate, part 4. The rapid descent of the drive shaft during an expansion as arrested when the thrust plate, part 28, strikes a one-half inch rubber pad mounted on the stop plate. The upper part of the drive shaft passes through a pressure seal into the interior of the cloud chamber, and ends supporting an aluminum sandwich, parts 23 and 24, which holds a rubber diaphragm. The diaphragm is anchored at its outer edge between the large mounting rings and near its center between small ridges on the aluminum plates. This leaves most of the diaphragm free to stretch during the motion of the piston, but the sandwich prevents all but a little ballooning at the outer one-half

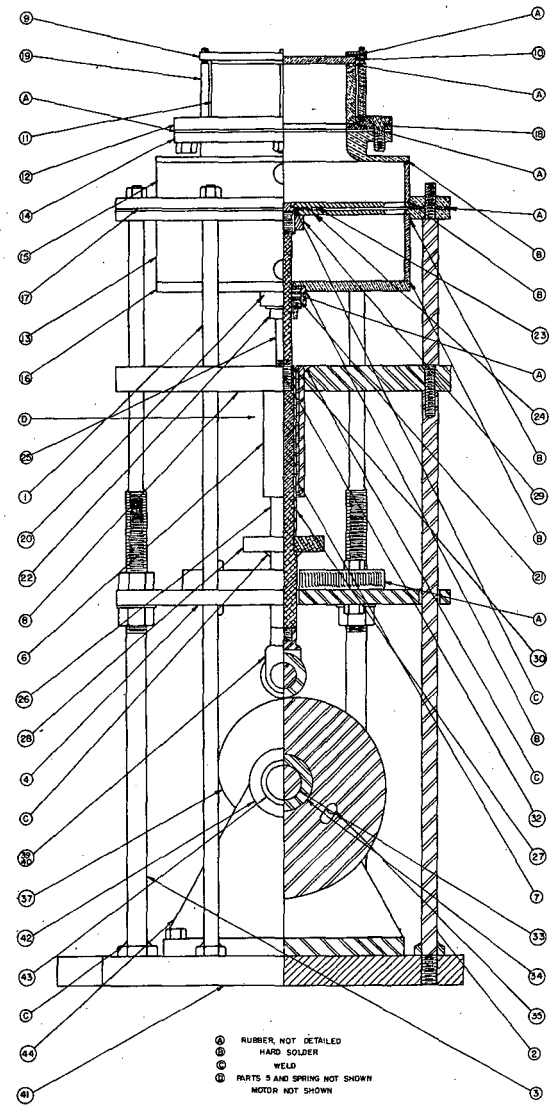
A RUBBER, NOT DETAILED
B HARD SOLDER
C WELD
D PARTS 5 AND SPRING NOT SHOWN
MOTOR NOT SHOWN
ASSEMBLY FROM DETAILS
MU3527

Fig. 16

inch. The small Lucite cylinder, part 11, represents the usable volume of the chamber. This diagram should be compared with the photograph, Figure 8.

Figures 17 through 21 are the original design drawings for the parts of the chamber. Certain changes were made during the construction. The following paragraphs supply explanatory material about the functions of several of these parts and enumerate the changes made. The numbers refer to the part numbers on the drawings.

2 and 3 — The overall length of these rods was increased to 14-3/4 inches and 5/8 inch of thread was applied to the right ends. A positioning nut was welded in place above the threads. These rods are shown correctly in the assembly drawing, Figure 16.

4 — The central hole was enlarged and fitted with an oilite bronze bearing to fit the guide shaft (part 26) and restrict the bending of the shaft under load.

10 — The cover glass thickness was increased to 3/16 inch.

11 — The grooves in the chamber wall are for O rings used to provide the pressure seal. The final chamber wall was as sketched except that two rectangular windows were cut, and 10 mil tantalum foil attached flush with the internal surface.

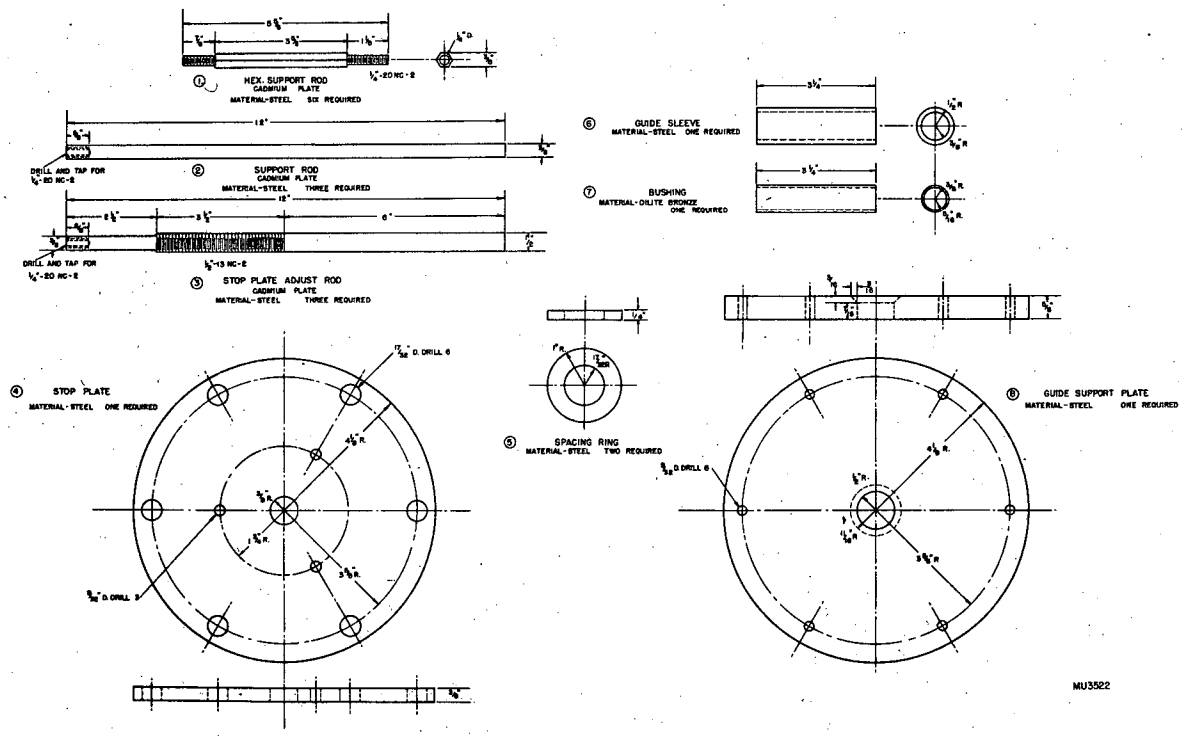
① HEX. SUPPORT ROD
CADMIUM PLATE
MATERIAL-STEEL SIX REQUIRED
② SUPPORT ROD
CADMIUM PLATE
MATERIAL-STEEL THREE REQUIRED
DRILL AND TAP FOR
DRILL AND TAP FOR
③ STOP PLATE ADJUST ROD
CADMIUM PLATE
MATERIAL-STEEL THREE REQUIRED
④ STOP PLATE
MATERIAL-STEEL ONE REQUIRED
⑤ SPACING RING
MATERIAL-STEEL TWO REQUIRED
⑥ GUIDE SLEEVE
MATERIAL-STEEL ONE REQUIRED
⑦ BUSHING
MATERIAL-OILITE BRONZE
ONE REQUIRED
⑧ GUIDE SUPPORT PLATE
MATERIAL-STEEL ONE REQUIRED
MU3522

Fig. 17

14 The undercut was eliminated and the holes threaded for 1/4-20.

18 A slot was cut in the head of the stud to allow tightening of the stud into part 14 with a screwdriver.

19 This was redesigned with an overall length of 2-1/16 inches, the left thread 9/16 inch long, and the unthreaded part 1-3/8 inches long.

20, 21, 22 These parts fit together to form the pressure seal. Rubber washers fit between the brass washers and bear against the moving shaft. See assembly.

26 (Mislabeled 25 on Figure 19). The 1/4-20 threaded portion was eliminated. Instead, the end of the shaft was drilled and tapped and a 3/8-16 threaded steel stud inserted. To this is attached the cam follower roller bearing assembly (Figure 20). All of the parts on Figure 19 fit together to form the main drive shaft. Part 23 is welded to part 25. Part 29 presses part 24 toward part 23 squeezing the rubber diaphragm at the center between the ridges. The diaphragm has a central hole that allows assembling over part 25.

34 The overall diameter was increased to 3-1/4 inches, and provision was made for only one torsion pin mounted on a circle of 2-3/4 inch diameter.

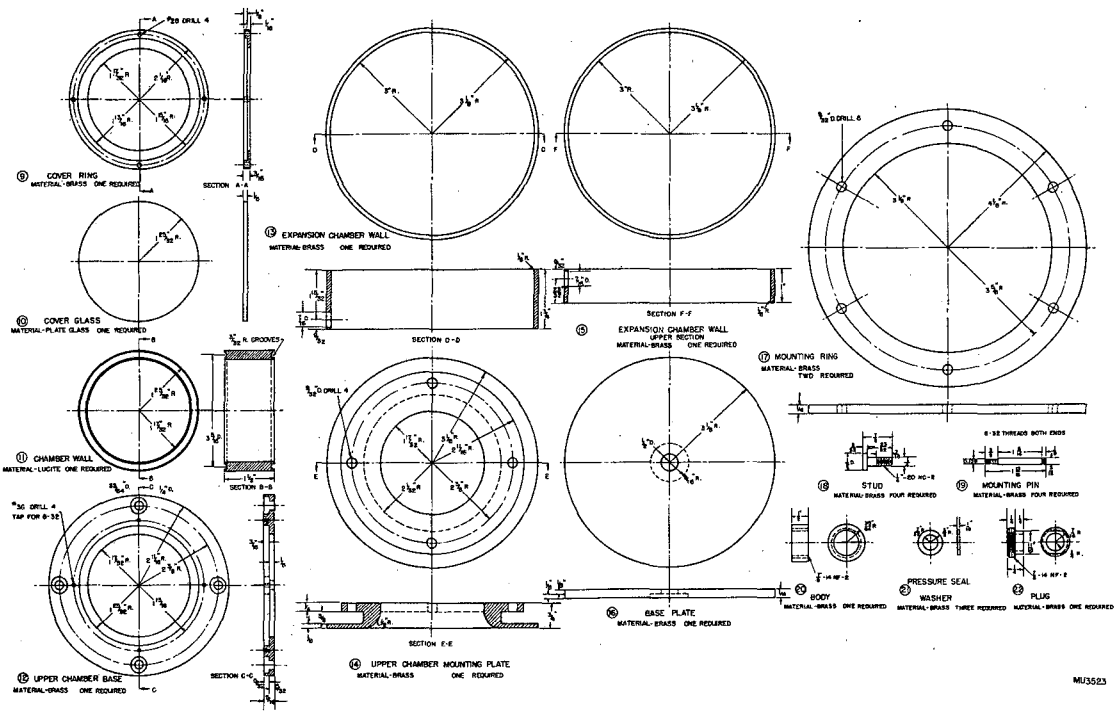
⑨ COVER RING
MATERIAL-BRASS ONE REQUIRED
SECTION A-A
⑩ COVER GLASS
MATERIAL-PLATE GLASS ONE REQUIRED
⑬ EXPANSION CHAMBER WALL
MATERIAL-BRASS ONE REQUIRED
SECTION D-D
SECTION F-F
⑮ EXPANSION CHAMBER WALL
UPPER SECTION
MATERIAL-BRASS ONE REQUIRED
⑰ MOUNTING RING
MATERIAL-BRASS
TWO REQUIRED
⑪ CHAMBER WALL
MATERIAL-LUCITE ONE REQUIRED
SECTION B-B
⑱ STUD
MATERIAL-BRASS FOUR REQUIRED
⑲ MOUNTING PIN
MATERIAL-BRASS FOUR REQUIRED
⑫ UPPER CHAMBER BASE
MATERIAL-BRASS ONE REQUIRED
SECTION C-C
⑭ UPPER CHAMBER MOUNTING PLATE
MATERIAL-BRASS ONE REQUIRED
SECTION E-E
⑯ BASE PLATE
MATERIAL-BRASS ONE REQUIRED
㉑ BODY
MATERIAL-BRASS ONE REQUIRED
㉒ PRESSURE SEAL
WASHER
MATERIAL-BRASS THREE REQUIRED
㉓ PLUG
MATERIAL-BRASS ONE REQUIRED
MU3523

Fig. 18

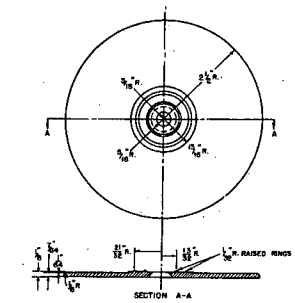

(23) DIAPHRAGM SUPPORT DISC
MATERIAL-ALUMINUM ONE REQUIRED

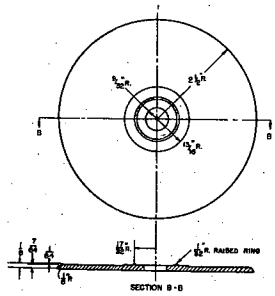

(24) DIAPHRAGM CLAMP PLATE
MATERIAL-ALUMINUM ONE REQUIRED

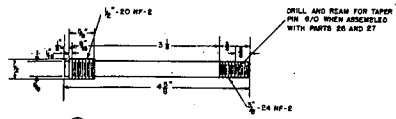

(25) SUPPORT SHAFT
MATERIAL-ALUMINUM ONE REQUIRED

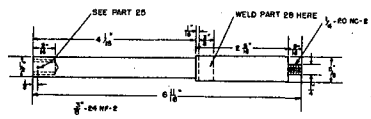

(25) GUIDE SHAFT
MATERIAL-ALUMINUM ONE REQUIRED

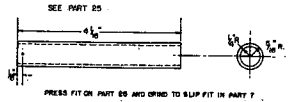

(27) GUIDE SHAFT BUSHING
MATERIAL-STEEL ONE REQUIRED

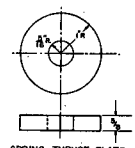

(28) SPRING THRUST PLATE
MATERIAL-ALUMINUM ONE REQUIRED

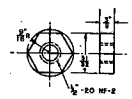

(29) CLAMP PLATE NUT
MATERIAL-ALUMINUM ONE REQUIRED

(30) LOCK NUT
MATERIAL-ALUMINUM ONE REQUIRED

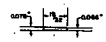

(32) TAPER PIN
MATERIAL-STEEL ONE REQUIRED

MU3524

Fig. 19

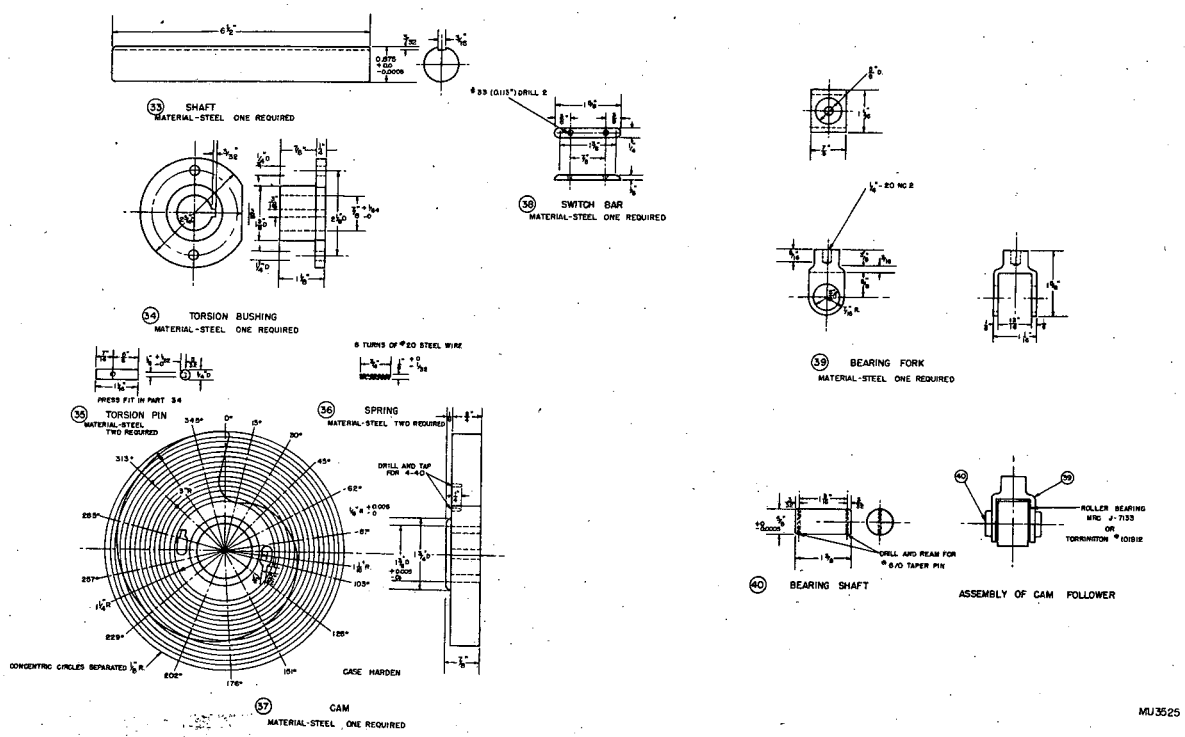
33 SHAFT
MATERIAL-STEEL ONE REQUIRED
30 SWITCH BAR
MATERIAL-STEEL ONE REQUIRED
34 TORSION BUSHING
MATERIAL-STEEL ONE REQUIRED
39 BEARING FORK
MATERIAL-STEEL ONE REQUIRED
35 TORSION PIN
MATERIAL-STEEL
TWO REQUIRED
36 SPRING
MATERIAL-STEEL TWO REQUIRED
6 TURNS OF #20 STEEL WIRE
PRESS FIT IN PART 34
DRILL AND TAP FOR 4-40
CONCENTRIC CIRCLES SEPARATED 1/8 R.
CASE HARDEN
37 CAM
MATERIAL-STEEL ONE REQUIRED
40 BEARING SHAFT
ROLLER BEARING
MRC J-7133
OR
TORRINGTON #10B12
DRILL AND REAM FOR #6/0 TAPER PIN
ASSEMBLY OF CAM FOLLOWER
MU3525

Fig. 20

35 Length was changed to 5/8 inch, the hole was eliminated, and only one pin was required.

36 Eliminated.

37 The slots for the torsion pin were moved out to accommodate the change made in part 34. The cuts in the end of these slots were eliminated. The cam was given a thorough cyanide hardening. The equation of this cam, in polar coordinates, is two quadratics joined smoothly in the center. The curve near the top is designed to prevent exceeding the maximum torque rating of the gear box while that near the center prevents exceeding the maximum allowable bending moment of the aluminum shaft.

39 Thread changed to 3/8-16 to match part 26.

40 Cotter pins were used instead of taper pins. The shaft was hardened to 60 minimum Rockwell "C" scale.

41 The base plate was made of aluminum. Instead of spot facing to the required drive shaft height of 4-3/8 inches and welding the bearing supports to the base, the bearing supports were welded to a separate block, 4-1/2 x 6 x 1/2 inches and the assembly bolted to the base. This modified assembly is shown in Figure 16.

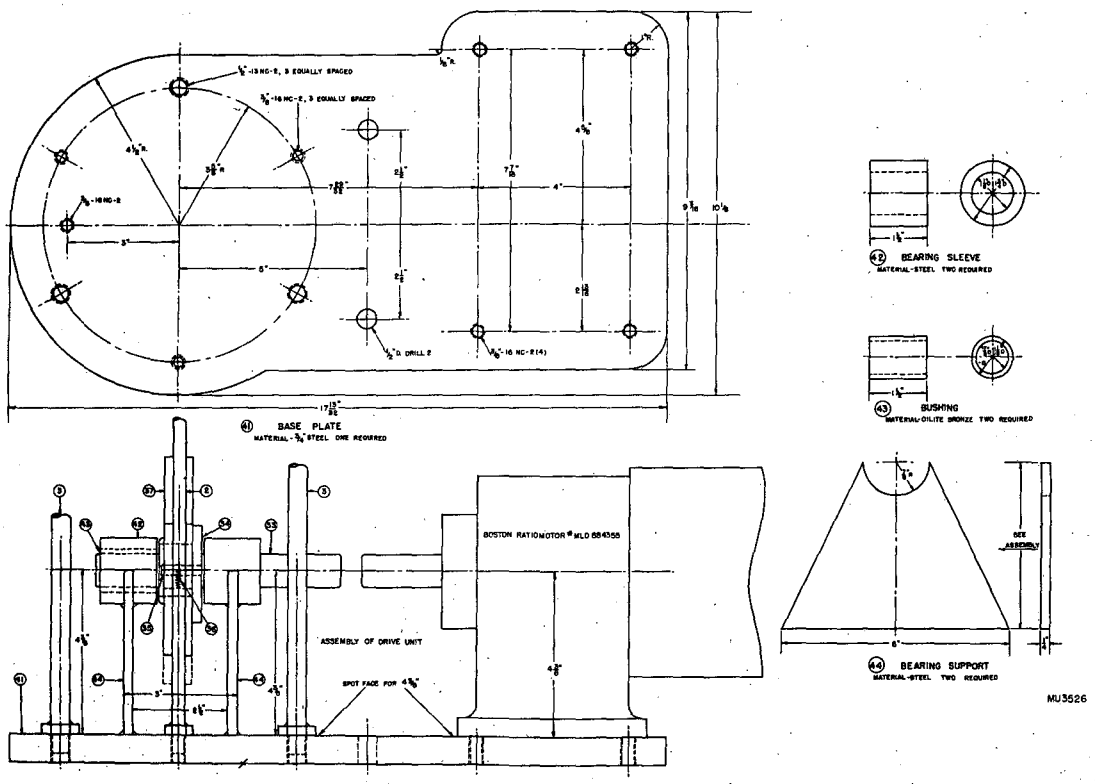
BASE PLATE
MATERIAL - STEEL ONE REQUIRED
BEARING SLEEVE
MATERIAL - STEEL TWO REQUIRED
BUSHING
MATERIAL - OILITE BRONZE TWO REQUIRED
BEARING SUPPORT
MATERIAL - STEEL TWO REQUIRED
BOSTON RATIOMOTOR MLD 684358
ASSEMBLY OF DRIVE UNIT
SPOT FACE FOR
SEE ASSEMBLY
MU3526

Fig. 21

All the joints are rubber gasketed, their position being indicated on the assembly drawing, but not detailed. A throttling pad consisting of seven layers of cheesecloth topped with black velvet and backed with copper screening was cemented in place with Vulcalock at the bottom of the chamber throat. To achieve a greater expansion ratio another top was constructed to replace the combination of parts 14, 15, and 17. This part had slanted internal walls to decrease the dead space in this tank. The change did not have great effect. The clearing field is horizontal. Thirty volts, balanced to ground, is applied between the two tantalum windows mounted in the chamber wall.

4.3 Chamber Performance. The expansion ratio is difficult to measure because of the presence of a high proportion of water vapor at the pressures used, compared with the total pressure. Measurements at different pressures are difficult to interpret because the diaphragm is flexible and responds differently to different pressure differences across it. The best estimate is believed to have been made when the chamber was compressed, the top removed and a measured amount of water poured in to fill it. The chamber was then expanded and the amount of water required to refill it measured. The weight of water will distort the diaphragm somewhat. Therefore this measurement is again only an approximation. The result gave an expansion ratio of 2.5 at the stop plate adjustment used for all work at low pressures. Because the effect of the throttling pad reduces the effective expansion ratio, the value two was adopted as an estimate of the net expansion ratio.

The speed of expansion was measured with an oscilloscope and wire probes set to intercept the motion of the thrust plate at the beginning and end of its motion. This measurement gave a value of three milliseconds.

The sensitive time of the chamber was measured by two methods. A plutonium alpha source of known counting rate was mounted in the chamber and a determination of the average number of recoils seen per picture was made. This measurement gave a value for the sensitive time of greater than seven milliseconds, the uncertainty due to the difficulty of estimating the total solid angle effectively seen. The second method was to observe the type of tracks obtained with various time delays of the light flash. Tracks do not occur in the photographs until the flashing of the light is delayed until the sensitive time begins. On the other hand if the flash is delayed until beyond the end of the sensitive time, all the tracks will appear diffuse. New tracks are very sharp. The technique was to photograph the chamber with the alpha source in it at various time delays. One then subtracts the minimum time delay that yields tracks from the maximum time delay that yields sharp, new tracks. This difference is the sensitive time. This method gave a result between ten and fifteen milliseconds. On this basis the sensitive time of the chamber has been assumed to be ten milliseconds.

The pressure range within which the chamber will operate satisfactorily is quite narrow, about 44 to 50 mm when 45 is the optimum. If the pressure goes too low the sensitive time becomes extremely short and

background condensation disappears entirely. When the pressure is increased, the background increases rapidly until, at a value 5 or 6 millimeters above the optimum value, a dense white cloud of extremely small droplets is formed. This narrow operating range is an advantage since one is assured that if tracks are being produced with little background, the density of the chamber cannot be far from its usual value. A slight temperature effect is observed, the optimum pressure rising about 1 mm/°C ambient temperature. Assuming an adiabatic expansion under typical conditions, one calculates a final pressure and temperature of 18 mm and -40° C, but these quantities do not mean very much in a chamber of this type. (See section 4.4)

Cloud chambers are subject to numerous annoying complaints. Fortunately a low pressure cloud chamber seems to be free of many of them. The one which has plagued the present development most regularly has been leaks. The presence of a very slight leak will admit enough unclean air to give convincing evidence of poisoning, but every case of apparent poisoning in this chamber has been traced to a leak from external air. The cloud chamber mechanism is an excellent pump, and the shock of every fast expansion provides an opportunity for entrance of a small amount of air either from the outside or from below the diaphragm. When designing and constructing such a chamber, one should emphasize protection from leaks.

Poisoning, turbulence, and radiation background are not problems in this chamber. The low pressure probably discriminates against poisoning agents of high vapor pressure. Reynolds' number is proportional

to the density, consequently turbulence problems are minimized at low pressure. Background due to cosmic or gamma rays is entirely absent since a particle of minimum ionization (70 ion pairs per inch in NTP air) will only make a dozen ion pairs in crossing the chamber, an amount indistinguishable from the slight general background.

The operation of the chamber is very reliable, and one can count on immediate operation, even after an extended period without operation.

4.4 Principles of Operation of Low Pressure Cloud Chambers.

1. Evaporation. In 1928 C. F. Powell[16] conducted a series of observations on a miniature glass expansion chamber to study its general behavior as a function of temperature and relative composition of the vapor. The chamber used water vapor and air in varying proportions. A paragraph from his paper will be quoted because its predictions have been very nicely demonstrated in the present work.

> Before the piston commences to fall the walls of the chamber are covered with a thin film of water, and the air throughout the chamber is saturated. As the piston moves the vapor expands, the air becomes unsaturated with respect to the water film, and this begins to evaporate. The amount of water evaporation during the expansion will depend on
>
> (a) the speed of the piston, and
> (b) the rate of diffusion of water vapor through the air.
>
> At high air pressures the rate of diffusion, which varies inversely as the air pressure, and the time of fall of the piston are both small, and but little water evaporates. Thus Wilson found his results independent of the size and speed of his expansion chamber when these were varied within wide limits. As the partial pressure of the air is reduced, however, the amount of evaporation during the expansion increases rapidly. The density of an element of the gaseous mixture in the middle of the expansion

> chamber does not change in the ratio V_2/V_1, and the lower the air pressure the greater the departure of the actual change in density from that deduced from the change in volume. Eventually a stage may be reached when, during the expansion, the total pressure in the chamber becomes less than the vapor pressure of the water on the walls. The evaporation will then be controlled not by the comparatively slow process of diffusion, but by the rate at which heat can be communicated to the surface of the liquid, by conduction from the interior of the film, to supply the latent heat of evaporation.

Powell calculates that for an expansion ratio of two in pure water vapor at 100° C, the vapor pressure will rise to normal value in 10^{-4} seconds. Something very similar is occuring in the present cloud chamber. The stopping power of the gas as calculated from the pressure measurements before the expansion and the known composition of the gas is 0.055 that of NTP air. This value cannot be as much as ten percent in error. The stopping power of the gas during the sensitive time is 0.076 that of NTP air, determinable accurately from the proton ranges to within ten percent. The density of the mixture has apparently increased. The final pressure of the gas after the sudden expansion, on the assumption of an adiabatic expansion of ratio two is 18 mm. Consequently it may be either a little above or below the boiling point of the water in the chamber, and the effect predicted by Powell may take place. Certainly the increase in stopping power must be due to evaporation of water, but there would seem to be a difficulty in the above hypothesis. If the evaporation takes place below the boiling point, the vapor must diffuse through the chamber, and even at these low pressures water vapor diffuses through air at only about one inch per second. The accelerator is pulsed nineteen

milliseconds after the beginning of the expansion. On the other hand if the vapor is boiled off the surface, it is difficult to understand how this large quantity of vapor rapidly evolved can be distributed promptly throughout the chamber without producing turbulence. Yet there is no turbulence present; fast proton tracks are perfectly straight.

A possible explanation is suggested by work done in 1924 by N. Gudris and L. Kulikova[17]. They investigated the rate of evaporation and growth of water drops by studying their rates of fall in a manner very similar to that used by Millikan in his oil-drop experiment. They found that drops of the order of 10^{-4} cm in diameter do not evaporate in nearly saturated air. They adsorb gas molecules on their surfaces and persist for hours. It seems perfectly possible that a cloud chamber is liberally supplied with such droplets when in operation. In a normal chamber where the total pressure does not change a great deal, these drops could be rather inert, their blanket of adsorbed gas impeding growth sufficiently to avoid fogging the chamber. (Reevaporation nuclei are believed to be about 10^{-7} cm radius). On the other hand, in a chamber of large expansion ratio and high percentage water vapor, the gas becomes very unsaturated with respect to these drops, and they could evaporate, providing a uniform and rapid rise of the gas density throughout the chamber.

Whatever the true explanation of this phenomenon is, the reevaporation of water is the most important feature of very low pressure chambers. This process reduces the supersaturation rapidly by carrying

heat into the gas and can easily render the chamber insensitive. For this reason a very rapid piston motion is of extreme importance in the operation of a low pressure chamber.

2. High Expansion Ratio. A chamber operating under the conditions described is far from adiabatic and it is necessary to draw considerably more work out of the expanding gas than in a standard chamber if it is to become cold enough to absorb the heat flowing into the chamber and maintain supersaturation.

3. Role of Permanent Gas. The permanent gas performs the functions of cooling the hot vapor evaporating into the chamber thereby maintaining supersaturation, and promoting condensation by removing the latent heat of condensation from forming drops. Experience with the present chamber shows that a rise in ambient temperature causing a rise in the vapor pressure of the water requires a rise in the total pressure of the gas. This indicates that with a given expansion ratio and piston speed a certain proportion of permanent gas is needed. An important function of the permanent gas (Powell[16]) is the restriction of reevaporation.

4. Short Sensitive Time. This effect, noted by Joliot[15], is a direct result of reevaporation, but it is not a completely unavoidable, intrinsic feature of a low pressure cloud chamber since it depends upon the piston speed. Joliot's sensitive time rises very little even with 200 mm of pressure before the expansion. The present chamber, with a short expansion time achieved five times as long a sensitive time.

4.5 Suggested Modifications. The present cloud chamber has functioned reliably, but did not go to as low a pressure as originally hoped. Powell[16] suggests running a pure vapor chamber barely saturated to avoid the reevaporation problem. This should be tried, but might be difficult to do in a chamber equipped with a throttling pad since it will tend to adsorb water. Another scheme, which is going to be tried with the present chamber, is to refrigerate it, thereby decreasing the water vapor pressure and maintaining a favorable ratio to the permanent gas pressure.

A few mechanical details should be improved on the chamber. The drive spring twists slightly when compressed, and this slowly rotates the roller bearing out of line with the cam, necessitating straightening it with a wrench every dozen or so cycles. A guide should be installed to prevent this rotation. The microswitch mount should be redesigned. The present one is hard to adjust and microswitch one must be provided with a stiffener since it is mounted in a reversed position. The rubber finger on the safety stop switch should be replaced with one of metal. Oil on the rubber softens it rendering the operation of the switch unreliable.

In designing a new chamber, it would be wise to design a drive spring with a longer travel than the one used here to enable a piston the same size as the cylinder of the sensitive volume to be used. Careful design to eliminate gas pockets can lead to a chamber which does not require slow cleaning expansions.

Chapter Five

Associated Control Electronics

5.1 Necessary Functions of Control System. The motor driven cam arrangement used to control the expansion of the chamber requires a time of the order of a second to begin the expansion after power is applied to the driving motor. Consequently it is not possible to expand the chamber on a signal from some established timing sequence in order to have it sensitive during one of the series of pulses from an accelerator. It is necessary to have the cloud chamber itself initiate the timing sequence. This is done by the momentary closing of a microswitch at the beginning of the expansion. As soon as the roller bearing reaches the edge of the cam and starts over, the tangential component of force on the cam causes it to shift completely out of the way and the piston is free to descend. The abrupt shift of the cam is very sudden, and the microswitch is adjusted so that the switch bar on the cam activates the switch near the end of this short path. This provides an accurate and reproducible time for the beginning of the timing cycle. The pulse must initiate the following events:

1. Short out the clearing field.
2. Pulse the accelerator at a controlled and variable delay time.
3. Flash the light at a controlled and variable delay time.
4. Restore the clearing field.

5. Advance the film in the camera.

6. Return the motor drive control system to its initial condition ready for a new cycle.

These must be done in this order, except number six can occur at any time during the sequence, and the relative order of 4 and 5 is unimportant.

The motor control system must carry out any one of a number of possible preset programs. The standard operating program is this:

1. The chamber gas is compressed.

2. A delay of several seconds in compressed position is made allowing the gas in the chamber to reach thermal equilibrium.

3. A slow expansion is made. (The motor reverses, and the roller bearing backs down the cam.)

4. The chamber is recompressed.

5. Step two is repeated.

6. The chamber is expanded ("popped").

7. Step one is repeated, and the cycle begins again.

In addition to the operating program, it is necessary to be able to set the program for continuous slow expansions without any pops, and to allow for more than one slow expansion between each fast expansion. There should be a signal to inform the operator that a fast expansion is imminent and a safety device to automatically cut the power to the motor should it go into reverse by accident when the chamber is expanded. If this should

occur, the flat edge of the cam will back into the roller bearing and inexorably bend the main shaft and break off the roller bearing. Provision must also be made for the operator to interrupt the control cycle at any point and take over manual control should the control system malfunction or some special behavior be required.

5.2 Time Delay and Associated Control Circuit. Figure 22 is the schematic for this part of the control system. Microswitch (1) is activated when the chamber begins the expansion. This pulse triggers the 6SN7 single-cycle multivibrator. Initially the left hand triode is conducting and the right cut off. The pulse initiates conduction in the right hand triode which lasts 0.6 seconds after which the circuit reverts to its initial condition. During the 0.6 second conduction period, the four relays whose coils are connected in series are closed. These relays are 5000 ohm sensitive relays which operate on about 8 ma.

The first relay, associated with the first 2050 thyratron, controls two functions. After a time delay, controllable between limits of 0.02 seconds to one-third of a second by the one Megohm potentiometer in the 0.5 μf grid condenser charging circuit, the thyratron fires and the 60 μf condenser discharges through a relay coil in the motor control system (described in paragraph 5.3) which resets that circuit to the beginning of the motor cycle. The second function (the one which requires the variable time delay) is to trigger the accelerator or other equipment requiring synchronization with the cloud chamber expansion. This output is taken from a potentiometer connected across the reset relay circuit.

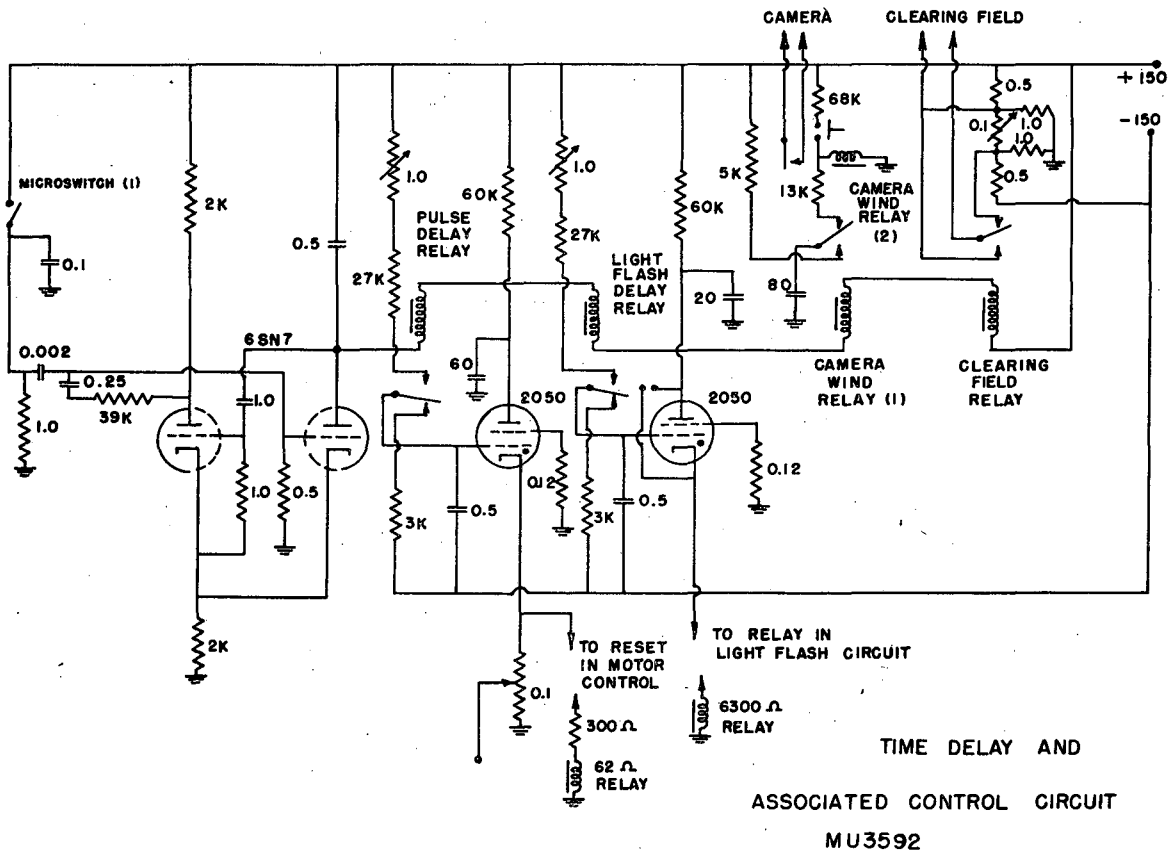

TIME DELAY AND ASSOCIATED CONTROL CIRCUIT MU3592

Fig. 22

This pulse was not used in the experiment reported in part one of this paper.

The second relay and thyratron form a very similar circuit to the first. In this case a 20 μf condenser is discharged through a 6300 ohm relay coil which flashes the light for photography (circuit discussed in paragraph 5.4). The thyratron is shunted with a push button to allow flashing the light at the will of the operator. The minimum time delay between the beginning of the expansion and the flashing of the light is about 30 milliseconds, ten milliseconds longer than the previous circuit, since the mechanical relay requires some time to close. When the four series relays reopen, the -150 volts applied to the grid is sufficient to cut off the small current through the thyratron which remains after the condenser is discharged.

When the third series relay closes, the 80 μf condenser is charged from the power supply through a 5000 ohm resistor. Then 0.6 seconds later, after the light has flashed and the photograph made, the relay opens and the condenser discharges with a longer time constant through the coil of a second relay, holding it closed for about four seconds. The film winding mechanism in the camera is driven by a motor. The motor is controlled by a film-measuring cam and microswitch which opens after a measured amount of film has passed. To wind the subsequent length of film into position, power must be applied to the motor for three or four seconds to allow it to rotate the cam and microswitch into closed position again. This four-second initiating power pulse is

supplied by this relay. A push button is provided for manual film advancing.

The fourth relay shorts out the clearing field to preserve sharp tracks when the chamber is sensitive after the expansion, and then reapplies the field after the photography is completed. The resistor network associated with this relay provides a variable clearing field voltage, balanced to ground for use in the horizontal clearing field used in this chamber. During several months of operation, none of the various functions of this circuit has ever been known to fail.

5.3 Motor Control System. The control of the cloud chamber drive motor is complicated by the requirement that the motor must go forward until the chamber is compressed, then stop and wait, reverse itself, back down to fully expanded position, come to a halt, and then go forward again. This cycle must be repeated a selected number of times until at the top of the compression the motor goes forward and the chamber is popped, after which the entire cycle must be repeated. The control system which accomplishes this is shown in Figure 23. The numbers (1) and (2) stand for the two sides of the 110 v. A.C. power line. The main features are:

Upper left, the Motor Start Relay. The power to the drive motor passes through the contacts of this relay. The Cycle Interrupt switch, normally closed, enables the operator to stop the motor at any time. A push button also allows him to run the motor at any time. The safety stop is a microswitch with a stiff rubber finger

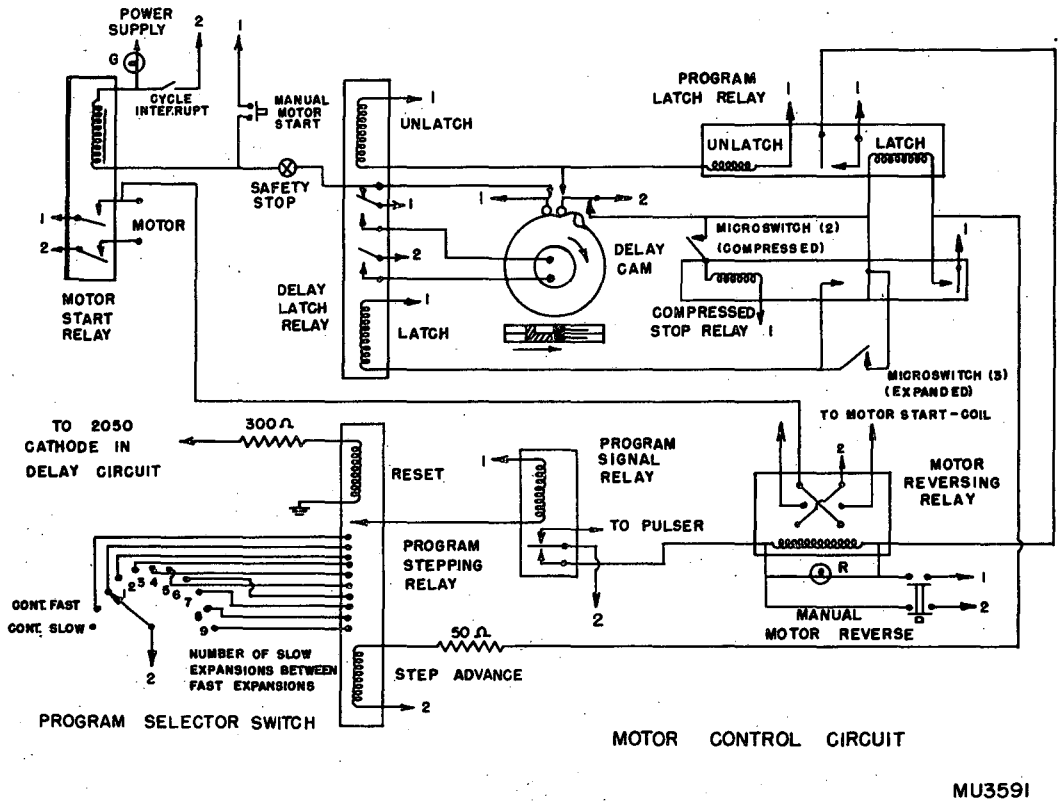
POWER SUPPLY
G
CYCLE INTERRUPT
MANUAL MOTOR START
SAFETY STOP
MOTOR
MOTOR START RELAY
DELAY LATCH RELAY
UNLATCH
LATCH
PROGRAM LATCH RELAY
UNLATCH
LATCH
DELAY CAM
MICROSWITCH (2) (COMPRESSED)
COMPRESSED STOP RELAY
MICROSWITCH (3) (EXPANDED)
TO MOTOR START-COIL
TO 2050 CATHODE IN DELAY CIRCUIT
300Ω
RESET
PROGRAM SIGNAL RELAY
TO PULSER
PROGRAM STEPPING RELAY
MOTOR REVERSING RELAY
R
MANUAL MOTOR REVERSE
CONT. FAST
CONT. SLOW
NUMBER OF SLOW EXPANSIONS BETWEEN FAST EXPANSIONS
50Ω
STEP ADVANCE
PROGRAM SELECTOR SWITCH
MOTOR CONTROL CIRCUIT
MU3591

Fig. 23

fastened at one end along the switch arm. This finger extends into the path of the top of the cam. The switch is normally closed. When the cam passes this switch traveling in the forward, or compressing direction, the finger is bent away from the switch arm out of the way and does nothing. On the other hand, should the motor become reversed at the wrong time and the flat cam face come swinging up towards the roller bearing, it will first encounter the rubber finger, push it against the switch arm, open the circuit, and stop the motor.

Upper center, motor driven Delay Cam. This provides a fixed delay of about eight seconds at the top and bottom of the piston motion to allow the motor to come to a halt and the gas in the chamber to come to thermal equilibrium.

Lower left, Program Stepping Relay. This controls the program of the cycle of operation. By adjusting the Program Selector Switch the operator can set for continuous slow expansions, continuous fast expansions, or interpose from one to nine slow expansions between each fast expansion.

Lower right, Motor Reversing Relay. When this relay is operated the connections to the motor start-winding are interchanged so that when power is applied, the motor will go into reverse. A red warning light warns the operator

that the motor will do this. A manual reversing push button is provided.

Information of the position of the cloud chamber piston is supplied to the control system by two microswitches operated by the same switch bar on the drive cam that operates microswitch one, which is the switch that triggers the time delay circuit discussed in section 5.2. Microswitch two closes when the piston reaches the top of its motion when the chamber is compressed. Since the motor is under load when this happens, the motor stops immediately when power is removed and microswitch two remains closed until the motor starts again. When the chamber is fully expanded the switch bar closes microswitch 3 momentarily, but the cam coasts on by and the switch reopens. These microswitches are shown on the diagram above and below the Compressed Stop Relay.

Let us examine the sequence of events when the Program Selector Switch is in the Continuous Slow position. When power is applied to the apparatus, the Motor Start Relay will close, power being supplied to its coil from line 2 through the normally closed cycle interrupt switch and from line 1 through the unlatched position of the Delay Latch Relay. The drive motor advances the cam until the chamber is compressed, closing microswitch 2. Since the switches on the motor driven Delay Cam are in their normal positions, the right hand switch is closed and line 2 is connected to microswitch 2. Therefore closing microswitch 2 causes the Compressed Stop Relay to close. The right hand contacts of this relay cause the stepping relay to advance one step, while the left hand contacts

simultaneously close and latch both the Program Latch Relay and the Delay Latch Relay. Consider the action of the former first. Its closing connects line 1 to one end of the coil of the Motor Reversing Relay. Line 2 is connected to the other end of this coil through the normally closed contact of the Program Signal Relay. Consequently the Motor Reversing Relay closes and remains closed as long as the Program Latch Relay is latched. The latching of the Delay Latch Relay removes power from the drive motor, which causes it to stop immediately leaving microswitch two closed, and applies power to the Delay Cam motor. The cam takes about eight seconds to make one revolution at the end of which the left hand switch is closed a fraction of a second before the right hand switch. This causes power to be applied to the motor and enables it to get started in reverse before the closing of the right hand switch unlatches the two latch relays thereby returning the Motor Reversing Relay to normal position. The unlatching of the Delay Latch Relay removes power from the motor driving the Delay Cam, and the cam coasts a small fraction of a revolution allowing both of its switches to return to their normal position.

The system is now in the same condition it was in at the beginning except that the stepping relay is advanced one position (which has no bearing on the operation when the Program Selector Switch is in Continuous Slow position) and the motor is running backwards producing a slow expansion of the cloud chamber. When the slow expansion is completed, the switch bar momentarily closes microswitch three which causes the Delay Latch Relay only to close and latch. This stops the drive motor and starts

the delay cam motor, but in this case the Motor Reversing Relay is not operated so that when the drive motor is reenergized, it will go forward. When the drive motor starts forward it again encounters microswitch three across which it has just coasted, so that a double delay is produced at the bottom of the cycle. Following the second delay a compression is begun and the cycle is complete.

With the Program Selector Switch in the Continuous Slow position, the above cycle is repeated indefinitely. To pop the chamber it is necessary to start the drive motor forward after it has stopped in the compressed position (microswitch 2 closed). To do this, the closing of the Motor Reversing Relay must be prevented. This is done by energizing the coil of the Program Signal Relay which opens the connection of line 2 to the coil of the Motor Reversing Relay. This is accomplished when the Program Stepping Relay reaches the contact to which line 2 has been connected through the Program Selector Switch. The operator is warned of the imminent fast expansion of the cloud chamber when it is compressed and the red panel light is not lighted. Further explanation of the operation of the control system with the Program Selector Switch in its other positions is not needed except for the remark that when the chamber pops, the circuit described in section 5.2 sends a pulse through the reset coil of the Program Stepping Relay to return it to its initial, open position.

Unlike the time delay circuit, the motor control system has not been entirely free from malfunctioning, although its failures have been in the form of annoyances rather than serious interference with the

proper sequence of operations. Its major trouble has been frequent failure of the stepping relay to return all the way to its initial position. This matter is discussed in section 5.5.

5.4 Power Supply. Figure 24 shows the various circuits used in the power supply, none of which is unusual. The power supply for the time delay circuit contains two half-wave rectifiers, one supplying +150 volts to ground, the other -150 volts. It is necessary to shunt one of the chokes with a 4000 ohm resistor to get a full 40 ma out of the supply regulated at 150 volts by the VR tube. It is necessary to leave the center tap of the heater transformer for the 6 x 4's ungrounded if excessive heater to cathode voltages are to be avoided.

The high voltage for the flash tube is provided by an 816 half-wave rectifier charging two 32 μf 2500 v. Pyranol Condensers from a 2000 v. transformer through a 20,000 ohm resistor to 2400 volts. The tickling voltage is provided by charging a 40 μf condenser with a selenium half-wave rectifier from the power line and then discharging this condenser through the primary of an automobile ignition coil.

A forty-second delay allows full heating of the rectifier cathodes before anode voltage is applied.

5.5 Suggested Modifications. At the time when the control circuits were being designed, experiments with the cloud chamber seemed to indicate that it would be necessary at times to use two or three slow expansions between each fast expansion. Consequently the stepping relay was adopted. Since the only one available at the time was a ten position relay and since

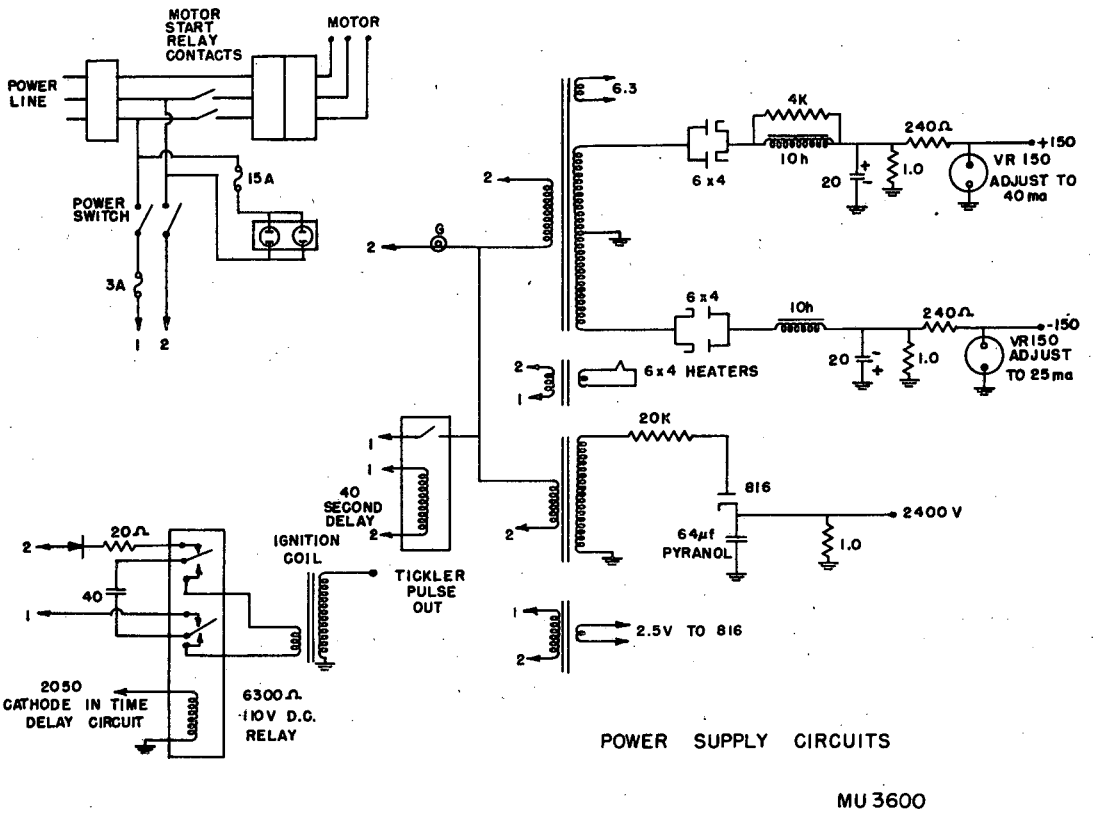
MOTOR START RELAY CONTACTS
MOTOR
POWER LINE
15A
POWER SWITCH
3A
1
2
6.3
4K
240Ω
+150
6x4
10h
20
1.0
VR 150
ADJUST TO 40 ma
6
6x4
10h
240Ω
-150
20
1.0
VR150 ADJUST TO 25 ma
6x4 HEATERS
20K
816
2400 V
64μf PYRANOL
1.0
2.5V TO 816
40 SECOND DELAY
IGNITION COIL
TICKLER PULSE OUT
20Ω
40
2050 CATHODE IN TIME DELAY CIRCUIT
6300Ω 110V D.C. RELAY
POWER SUPPLY CIRCUITS
MU 3600

Fig. 24

no harm was done by using its full capacity, the circuit shown was adopted giving a possibility of nine slow expansions. Subsequent improvement of the chamber and operating experience have shown that one slow expansion between pops is quite adequate. Furthermore it is not feasible to operate without slow expansions. This means that there are only two necessary operating programs, continuous slow expansions and alternate slow and fast expansions. A worthwhile circuit modification would be to replace the Program Selector Switch (11-position rotary) with a simple 2 position toggle switch to select the proper program and replace the stepping relay with simpler relays.

The Program Stepping Relay has been the principal source of trouble in this circuit since it frequently fails to reset completely. This does not interrupt the sequence of operation but it does require the operator to reset the switch position after most of the expansions. About once in every hundred cycles, the control system makes an error, and the motor starts up in reverse at the bottom of the cycle. Only the presence of the Safety Stop switch or an alert operator prevents disaster.

5.6 Van de Graaff Pulser. Figure 25 is the circuit diagram of the apparatus used to provide timing control for the Van de Graaff. Its function is to deliver a single triggering pulse at an adjustable delay following a trigger signal. The triggering pulse is formed by discharging the 0.5 μf condenser charged to 270 volts through the 2050 thyratron in series with a 500 ohm resistor. The output signal is taken from across this resistor. Initially the thyratron has a grid potential of -55 volts and

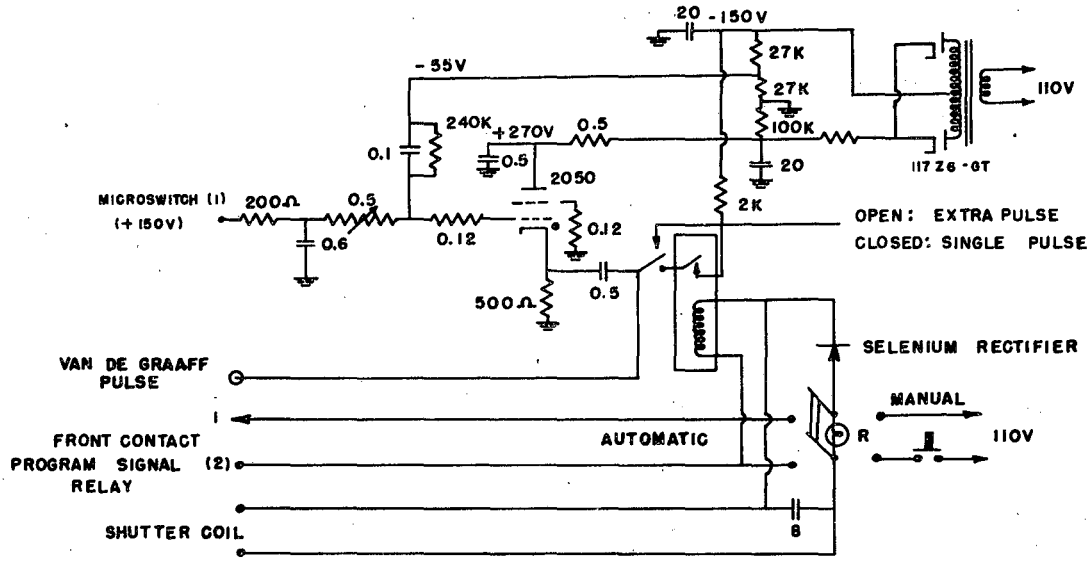

VAN DE GRAAFF PULSER

MU 3599

Fig. 25

is cut off. At the beginning of the cycle, the 0.6 μf condenser is charged almost immediately to +150 volts from a low impedance source (applied through microswitch one on the cloud chamber). The charge on this condenser then leaks through the adjustable half-megohm control to charge the 0.1 μf condenser. When the grid potential rises high enough, the tube fires. Since the condenser is shunted with a 0.24 megohm resistor, the range of time delays available is extended since the delay time increases sharply when the adjustable resistance is advanced to values greater than 0.24 megohm. The circuit will accurately reproduce delays ranging from 30 microseconds to 0.1 second. Figure 26 shows a plot of the delay versus dial setting of the potentiometer. The scale is a logarithmic scale from 110 down to 2 milliseconds, and linear from there to zero. For each abscissa, three independent measurements of the delay are shown. For the expanded region, two independent measurements are shown. The delays were measured with a Berkeley Interval Timer with resolving time of ten microseconds.

In operation, this circuit is associated with the circuits described in sections 5.2 and 5.3. It was found necessary to include the small resistor in series with the 0.6 μf condenser to allow reliable simultaneous triggering of the other control circuits from microswitch one. When the D.P.D.T. switch is in automatic position, power is applied to this part of the circuit only when the drive motor starts up in the <u>forward</u> direction when the chamber is compressed, i.e., just before a fast expansion. This opens the shutter (see Figure 9) allowing the proton

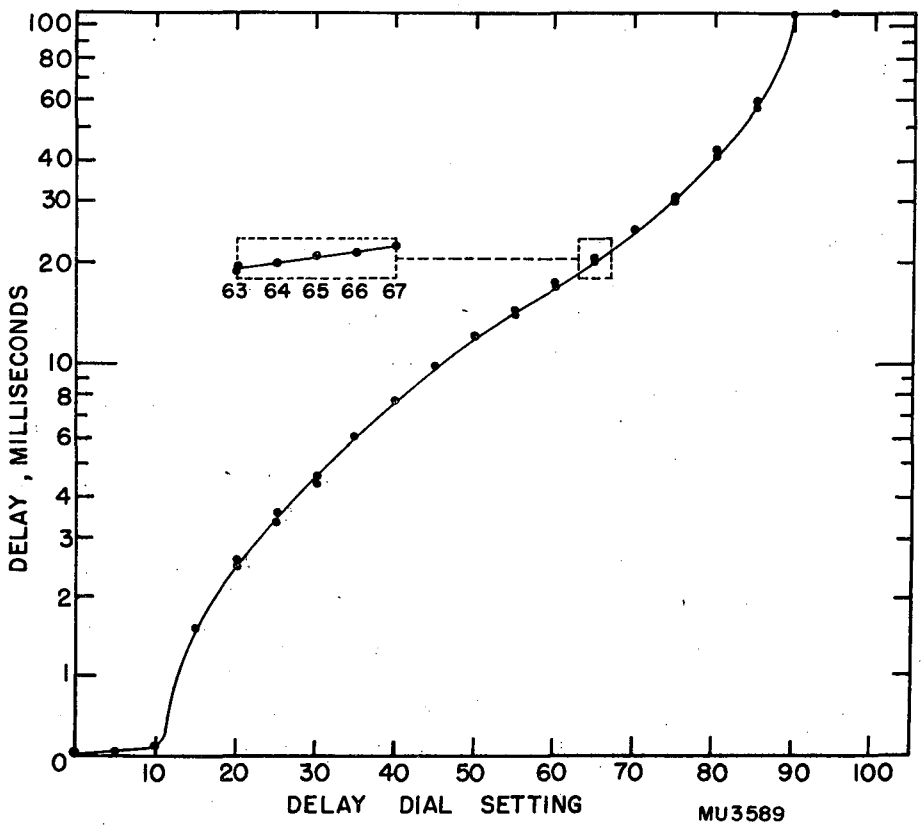
100
80
60
40
30
20
10
8
6
4
3
2
1
0
DELAY , MILLISECONDS
63 64 65 66 67
10 20 30 40 50 60 70 80 90 100
DELAY DIAL SETTING
MU3589

Fig. 26

beam to strike the lithium target, and also closes the relay shown in this circuit.

The control may be operated in two ways. If the S.P.S.T. switch is closed, in Single Pulse position, the closing of the relay puts -150 volts on the control line which stops the regular 15 pulses per second to the Van de Graaff, and the delayed pulse is alone. If the switch is opened, in Extra Pulse position, the regular pulses continue as usual and the controlled pulse is inserted as an extra one in the series. The latter mode of operation proved more successful because if the regular pulses are interrupted, the Van de Graaff voltage begins to rise, and reliable proton energy control becomes difficult.

With the D.P.D.T. switch in Manual position, the operator has pushbutton control on target bombardment. The red pilot light lights whenever the target is being bombarded.

Acknowledgements

The writer wishes to express his gratitude to Professor L. W. Alvarez whose original suggestion led to the problem. Professor Alvarez's continued interest and advice has been both helpful and encouraging. The writer also wishes to thank Professor Wilson Powell, who has welcomed him into the UCRL cloud chamber group and allowed him to make full use of all its facilities. Professor Powell has been interested in the problem and numerous discussions with him have been very helpful.

The help and cooperation of many people go into the simplest of research projects. In particular should be mentioned Mr. L. Edwards who did an excellent job of machine work in building the chamber. Mr. Alcalde and Mr. Edwards operate a very efficient shop in Building 50, and they both have been very willing to go out of their way to do unusual machine work promptly.

Mrs. Dorothy Gardner has done most of the Photographic processing required by this program, and Mrs. Beverly Lee spent long hours doing most of the tedious calculations involved in preparing the data in Appendices I and II. Mr. R. Finke of the linear accelerator crew gave up many of his free Saturdays in order to operate the Van de Graaff for the various runs. To all these people and numerous others the writer is indebted.

Appendix I

Figure 11 shows the neutron energies available from proton bombardment of lithium with protons of 2.5 Mev or less. This appendix presents the calculated energies used to draw the graph. The calculation is based on conservation of energy and momentum and may be done in the following form presented by Taschek and Hemmendinger[12] corrected for a better value of the threshold than available to them. The threshold chosen is 1.882 Mev as reported by Herb, Snowden, and Sala[11].

$$E_n = A^2 + B^2 + 2\,AB\cos\Phi$$

where

$$A = 0.1256\sqrt{E_p}$$

$$B = 0.8744\sqrt{E_p - 1882}$$

$$\Phi = \theta + \sin^{-1}\left(\frac{A\sin\theta}{B}\right)$$

E_n and E_p are the energies of the neutron and proton in kilovolts, and θ is the angle of production.

For a proton energy of 1900 kilovolts, the neutron energy is double-valued as follows:

	θ \ E_n	Low	High
	0°	3.12	84.36
	7.5°	3.20	82.23
	15.0°	3.47	75.98
	22.5°	3.99	65.93
	30.0°	5.01	52.49
	37.5°	7.37	35.67
Max.	42°39'24"	16.21	

For the other proton energies calculated, the neutron energies are single-valued and are tabulated on the following page.

θ \ E_p	1950	2000	2050	2100	2150	2200	2250	2300	2350	2400	2450	2500
0.0°	162.74	228.28	289.69	348.43	405.56	461.56	516.70	571.23	625.23	679.05	732.03	784.98
7.5	160.61	225.97	287.21	345.78	402.74	458.58	513.57	567.89	621.79	675.46	728.30	781.11
15.0	154.35	219.21	279.91	337.97	394.44	449.80	504.32	558.19	611.64	664.87	717.28	769.66
22.5	144.37	208.39	268.19	325.62	381.06	435.62	489.38	542.55	595.22	647.73	699.42	751.10
30.0	131.32	194.14	252.68	308.72	363.25	416.72	469.43	521.57	573.23	624.76	675.48	726.20
37.5	116.03	177.26	234.20	288.74	341.84	393.96	445.34	496.20	546.61	596.91	646.42	695.96
45.0	99.46	158.69	213.67	266.41	317.83	368.32	418.14	467.49	516.42	565.28	613.37	661.51
52.5	82.61	139.39	192.08	242.74	292.20	340.85	388.91	436.54	483.80	531.03	577.52	624.10
60.0	66.44	120.34	170.33	218.66	265.97	312.57	358.68	404.44	449.88	495.34	540.09	584.97
67.5	51.78	102.15	149.29	195.08	240.05	284.47	328.50	372.26	414.10	459.33	502.25	545.32
75.0	39.21	85.63	129.63	172.71	215.22	257.34	299.20	340.87	382.37	424.00	465.01	506.22
82.5	29.03	71.13	111.81	152.08	192.06	231.84	271.48	311.04	350.50	390.15	429.93	468.57
90.0	21.23	58.79	96.11	133.55	170.99	208.42	245.86	283.31	320.74	358.43	395.60	433.08
97.5	15.52	48.60	82.62	117.28	152.23	187.39	222.65	258.05	293.51	329.29	364.62	400.28
105.0	11.50	40.38	71.26	103.27	135.93	168.64	202.02	235.47	269.04	303.01	336.56	370.51
112.5	8.70	33.88	61.88	91.43	121.81	152.70	184.00	215.61	247.43	279.71	311.61	343.94
120.0	6.78	28.80	54.23	81.57	109.94	138.98	168.51	198.45	228.66	259.38	289.77	320.63
127.5	5.46	24.86	48.10	73.48	100.07	127.44	155.42	183.87	212.63	241.96	271.00	300.53
135.0	4.53	21.87	43.23	66.95	92.00	117.94	144.55	171.69	199.20	227.31	255.16	283.54
142.5	3.88	19.60	39.45	61.77	85.54	110.26	135.72	161.75	188.20	215.27	242.11	269.50
150.0	3.43	17.91	36.56	57.78	80.50	104.24	129.13	153.89	179.45	205.68	231.69	258.28
157.5	3.12	16.70	34.45	54.81	76.74	99.72	123.51	147.92	172.83	198.39	223.76	249.72
165.0	2.92	15.89	33.00	52.77	74.13	96.58	119.85	143.78	168.19	193.28	218.19	243.70
172.5	2.81	15.42	32.16	51.58	72.60	94.72	117.69	141.32	165.44	190.25	214.88	240.12
180.0	2.77	15.27	31.89	51.19	72.10	94.12	116.98	140.51	164.53	189.25	213.79	238.94

Appendix II

Figure 13 is a nomograph, or alignment chart, of the function $E = E_o \cos^2 \theta$. Since this is a commonly needed expression in scattering problems, the calculated values are tabulated. The overall dimensions of the nomograph are sketched here.

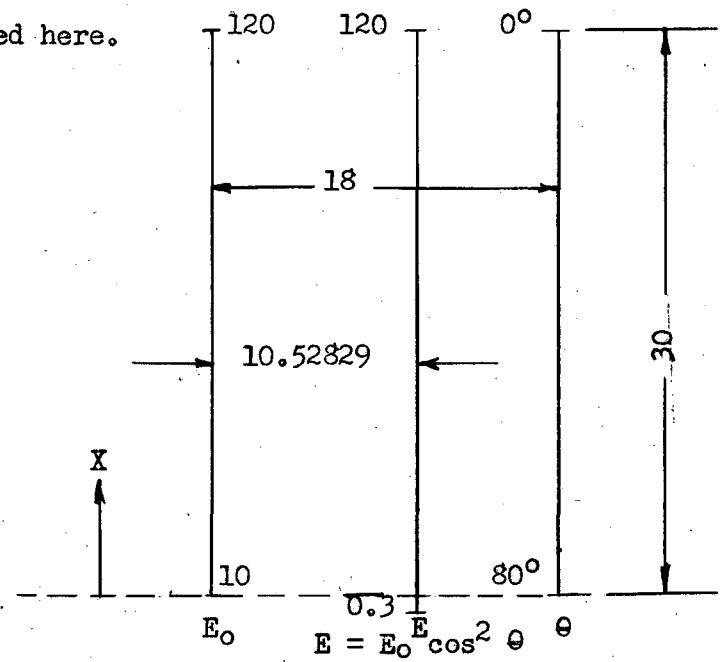

With the following tabulated data a nomograph of any size may be constructed with emphasis on any particular range of values desired. The chart may be magnified or reduced linearly in any direction. The scales may be moved vertically with respect to each other as long as one preserves the same triple of numbers intersected by a straight line across the three scales. This is done by fixing one scale and moving each one of the other two an amount proportional to its distance from the fixed scale. Each scale is tabulated separately with the calibration values paired with the corresponding distances, X, from the base line. These distances have been calculated with sufficient accuracy to allow considerable enlargement of the chart in order to emphasize a small part of it.

E_o	X	E_o	X	E_o	X	E_o	X	E_o	X
10.0	0.000	15.6	5.368	24.2	10.670	44.5	18.024	82	25.386
10.1	0.120	15.8	5.522	24.4	10.769	45.0	18.159	83	25.550
10.2	0.239	16.0	5.674	24.6	10.868	45.5	18.292	84	25.694
10.3	0.357	16.2	5.824	24.8	10.965	46.0	18.434	85	25.837
10.4	0.473	16.4	5.972	25.0	11.062	46.5	18.554	86	25.978
10.5	0.589	16.6	6.119	25.5	11.301	47.0	18.684	87	26.118
10.6	0.708	16.8	6.263	26.0	11.536	47.5	18.811	88	26.256
10.7	0.817	17.0	6.406	26.5	11.766	48.0	18.938	89	26.392
10.8	0.929	17.2	6.548	27.0	11.991	48.5	19.063	90	26.527
10.9	1.037	17.4	6.687	27.5	12.230	49.0	19.187	91	26.660
11.0	1.151	17.6	6.825	28.0	12.431	49.5	19.310	92	26.792
11.1	1.257	17.8	6.961	28.5	12.644	50.0	19.431	93	26.923
11.2	1.368	18.0	7.096	29.0	12.854	51.0	19.670	94	27.052
11.3	1.476	18.2	7.230	29.5	13.060	52.0	19.904	95	27.180
11.4	1.582	18.4	7.362	30.0	13.263	53.0	20.134	96	27.306
11.5	1.687	18.6	7.492	30.5	13.463	54.0	20.360	97	27.431
11.6	1.792	18.8	7.621	31.0	13.659	55.0	20.581	98	27.555
11.7	1.896	19.0	7.749	31.5	13.852	56.0	20.799	99	27.678
11.8	1.979	19.2	7.875	32.0	14.043	57.0	21.012	100	27.799
11.9	2.100	19.4	8.001	32.5	14.230	58.0	21.223	101	27.919
12.0	2.201	19.6	8.124	33.0	14.414	59.0	21.429	102	28.038
12.1	2.302	19.8	8.247	33.5	14.596	60.0	21.632	103	28.156
12.2	2.401	20.0	8.368	34.0	14.775	61.0	21.831	104	28.272
12.3	2.499	20.2	8.488	34.5	14.951	62.0	22.028	105	28.388
12.4	2.597	20.4	8.607	35.0	15.125	63.0	22.221	106	28.507
12.5	2.694	20.6	8.725	35.5	15.296	64.0	22.411	107	28.616
12.6	2.790	20.8	8.842	36.0	15.465	65.0	22.598	108	28.728
12.7	2.886	21.0	8.957	36.5	15.631	66.0	22.782	109	28.836
12.8	2.980	21.2	9.072	37.0	15.795	67.0	22.964	110	28.950
12.9	3.074	21.4	9.185	37.5	15.957	68.0	23.145	111	29.056
13.0	3.167	21.6	9.297	38.0	16.117	69.0	23.319	112	29.167
13.2	3.352	21.8	9.409	38.5	16.275	70.0	23.493	113	29.275
13.4	3.533	22.0	9.519	39.0	16.431	71.0	23.664	114	29.381
13.6	3.712	22.2	9.628	39.5	16.585	72.0	23.833	115	29.486
13.8	3.888	22.4	9.737	40.0	16.737	73.0	23.999	116	29.591
14.0	4.062	22.6	9.844	40.5	16.887	74.0	24.164	117	29.695
14.2	4.234	22.8	9.950	41.0	17.035	75.0	24.326	118	29.778
14.4	4.402	23.0	10.056	41.5	17.181	76.0	24.486	119	29.899
14.6	4.569	23.2	10.160	42.0	17.326	77.0	24.644	120	30.000
14.8	4.733	23.4	10.264	42.5	17.469	78.0	24.799		
15.0	4.895	23.6	10.366	43.0	17.610	79.0	24.953		
15.2	5.055	23.8	10.468	43.5	17.749	80.0	25.105		
15.4	5.213	24.0	10.569	44.0	17.887	81.0	25.255		

E	X	E	X	E	X	E	X	E	X
0.30	-0.026	0.90	5.479	3.0	11.512	10.0	17.545	35	23.823
0.31	+0.139	0.92	5.590	3.1	11.677	10.5	17.790	36	23.964
0.32	0.298	0.94	5.697	3.2	11.836	11.0	18.023	37	24.101
0.33	0.452	0.96	5.803	3.3	11.990	11.5	18.246	38	24.235
0.34	0.602	0.98	5.906	3.4	12.140	12.0	18.459	39	24.365
0.35	0.747	1.00	6.007	3.5	12.285	12.5	18.663	40	24.492
0.36	0.888	1.05	6.252	3.6	12.426	13.0	18.860	41	24.616
0.37	1.025	1.10	6.485	3.7	12.563	13.5	19.049	42	24.736
0.38	1.159	1.15	6.708	3.8	12.697	14.0	19.231	43	24.854
0.39	1.289	1.20	6.921	3.9	12.827	14.5	19.407	44	24.969
0.40	1.416	1.25	7.125	4.0	12.954	15.0	19.577	45	25.082
0.41	1.540	1.30	7.322	4.1	13.078	15.5	19.741	46	25.192
0.42	1.660	1.35	7.511	4.2	13.198	16.0	19.900	47	25.300
0.43	1.778	1.40	7.693	4.3	13.316	16.5	20.055	48	25.405
0.44	1.893	1.45	7.869	4.4	13.431	17.0	20.204	49	25.509
0.45	2.006	1.50	8.039	4.5	13.544	17.5	20.350	50	25.610
0.46	2.116	1.55	8.203	4.6	13.654	18.0	20.491	52	25.806
0.47	2.224	1.60	8.362	4.7	13.762	18.5	20.628	54	25.996
0.48	2.329	1.65	8.517	4.8	13.867	19.0	20.762	56	26.178
0.49	2.433	1.70	8.675	4.9	13.971	19.5	20.892	58	26.354
0.50	2.534	1.75	8.812	5.0	14.072	20.0	21.019	60	26.524
0.51	2.633	1.80	8.953	5.2	14.268	20.5	21.142	62	26.688
0.52	2.730	1.85	9.090	5.4	14.458	21.0	21.263	64	26.847
0.53	2.826	1.90	9.224	5.6	14.640	21.5	21.381	66	27.001
0.54	2.920	1.95	9.354	5.8	14.816	22.0	21.496	68	27.151
0.55	3.012	2.00	9.481	6.0	14.986	22.5	21.609	70	27.296
0.56	3.102	2.05	9.604	6.2	15.150	23.0	21.719	72	27.437
0.57	3.190	2.10	9.725	6.4	15.309	23.5	21.827	74	27.574
0.58	3.278	2.15	9.843	6.6	15.463	24.0	21.932	76	27.708
0.59	3.363	2.20	9.958	6.8	15.613	24.5	22.036	78	27.838
0.60	3.448	2.25	10.071	7.0	15.758	25.0	22.137	80	27.965
0.62	3.612	2.30	10.181	7.2	15.899	25.5	22.236	82	28.089
0.64	3.771	2.35	10.289	7.4	16.036	26.0	22.333	84	28.210
0.66	3.925	2.40	10.394	7.6	16.170	26.5	22.429	86	28.328
0.68	4.075	2.45	10.498	7.8	16.300	27.0	22.522	88	28.443
0.70	4.220	2.50	10.599	8.0	16.427	27.5	22.621	90	28.555
0.72	4.361	2.55	10.698	8.2	16.551	28.0	22.705	95	28.826
0.74	4.498	2.60	10.795	8.4	16.672	28.5	22.793	100	29.083
0.76	4.632	2.65	10.891	8.6	16.790	29.0	22.880	105	29.328
0.78	4.762	2.70	10.984	8.8	16.905	29.5	22.966	110	29.561
0.80	4.889	2.75	11.076	9.0	17.017	30.0	23.050	115	29.784
0.82	5.013	2.80	11.167	9.2	17.128	31.0	23.215	120	30.000
0.84	5.134	2.85	11.255	9.4	17.235	32.0	23.374		
0.86	5.252	2.90	11.342	9.6	17.341	33.0	23.528		
0.88	5.367	2.95	11.428	9.8	17.444	34.0	23.678		

θ	X	θ	X	θ	X	θ	X	θ	X
80.0°	0.000	72.4°	9.503	64.8°	15.370	57.2°	19.497	41.5°	25.046
79.8	0.337	72.2	9.692	64.6	15.496	57.0	19.588	41.0	25.177
79.6	0.664	72.0	9.877	64.4	15.622	56.8	19.678	40.5	25.306
79.4	0.988	71.8	10.059	64.2	15.744	56.6	19.769	40.0	25.433
79.2	1.304	71.6	10.240	64.0	15.867	56.4	19.860	39.5	25.557
79.0	1.615	71.4	10.418	63.8	15.989	56.2	19.950	39.0	25.679
78.8	1.919	71.2	10.595	63.6	16.111	56.0	20.039	38.5	25.799
78.6	2.219	71.0	10.769	63.4	16.230	55.8	20.128	38.0	25.917
78.4	2.515	70.8	10.943	63.2	16.352	55.6	20.215	37.5	26.033
78.2	2.803	70.6	11.112	63.0	16.466	55.4	20.302	37.0	26.147
78.0	3.087	70.4	11.282	62.8	16.585	55.2	20.389	36.5	26.258
77.8	3.367	70.2	11.452	62.6	16.699	55.0	20.474	36.0	26.368
77.6	3.639	70.0	11.617	62.4	16.818	54.5	20.686	35.5	26.476
77.4	3.908	69.8	11.779	62.2	16.928	54.0	20.894	35.0	26.581
77.2	4.176	69.6	11.941	62.0	17.043	53.5	21.098	34.5	26.685
77.0	4.436	69.4	12.099	61.8	17.153	53.0	21.298	34.0	26.787
76.8	4.693	69.2	12.260	61.6	17.268	52.5	21.495	33.5	26.887
76.6	4.945	69.0	12.414	61.4	17.378	52.0	26.688	33.0	26.985
76.4	5.194	68.8	12.572	61.2	17.484	51.5	21.878	32.5	27.081
76.2	5.439	68.6	12.722	61.0	17.595	51.0	22.064	32.0	27.175
76.0	5.683	68.4	12.876	60.8	17.702	50.5	22.247	31.5	27.268
75.8	5.920	68.2	13.026	60.6	17.808	50.0	22.427	31.0	27.359
75.6	6.157	68.0	13.176	60.4	17.915	49.5	22.603	30.5	27.448
75.4	6.386	67.8	13.322	60.2	18.017	49.0	22.777	30.0	27.535
75.2	6.612	67.6	13.468	60.0	18.124	48.5	22.947	29.0	27.704
75.0	6.839	67.4	13.614	59.8	18.226	48.0	23.115	28.0	27.866
74.8	7.060	67.2	13.756	59.6	18.329	47.5	23.279	27.0	28.022
74.6	7.281	67.0	13.898	59.4	18.432	47.0	23.441	26.0	28.171
74.4	7.494	66.8	14.036	59.2	18.530	46.5	23.600	25.0	28.314
74.2	7.707	66.6	14.178	59.0	18.629	46.0	23.756	24.0	28.450
74.0	7.916	66.4	14.312	58.8	18.731	45.5	23.910	23.0	28.580
73.8	8.126	66.2	14.450	58.6	18.826	45.0	24.061	22.0	28.704
73.6	8.331	66.0	14.584	58.4	18.925	44.5	24.209	21.0	28.822
73.4	8.532	65.8	14.719	58.2	19.023	44.0	24.355	20.0	28.934
73.2	8.729	65.6	14.853	58.0	19.118	43.5	24.498	15.0	29.405
73.0	8.926	65.4	14.983	57.8	19.213	43.0	24.639	10.0	29.737
72.8	9.124	65.2	15.113	57.6	19.307	42.5	24.777	5.0	29.934
72.6	9.313	65.0	15.239	57.4	19.402	42.0	24.912	0.0	30.000

Bibliography

1. N. Bohr. Phys. Rev. 59, 270 (1941).
2. P. M. S. Blackett. Proc. Roy. Soc. A 103, 62 (1923).
3. P. M. S. Blackett and D. S. Lees. Proc. Roy. Soc. A 134, 658 (1932).
4. W. W. Eaton. Phys. Rev. 48, 921 (1935).
5. R. L. Anthony. Phys. Rev. 50, 726 (1936).
6. J. T. McCarthy. Phys. Rev. 53, 30 (1938).
7. G. A. Wrenshall. Phys. Rev. 57, 1095 (1940).
8. M. S. Livingston and H. A. Bethe. Rev. Mod. Phys. 9, 261 (1937).
9. H. A. Bethe. Rev. Mod. Phys. 22, 213 (1950).
10. K. Brueckner, W. Hartsough, E. Hayward and W. M. Powell. Phys. Rev. 75, 555 (1949).
11. R. G. Herb, S. C. Snowden and O. Sala. Phys. Rev. 75, 246 (1949).
12. R. Taschek and A. Hemmendinger. Phys. Rev. 74, 373 (1948).
13. C. M. Crenshaw. Phys. Rev. 62, 54 (1942).
14. W. A. Aron, B. G. Hoffman and F. C. Williams. UCRL-121.
15. F. Joliot. J. de Phys. Rad. 5, 216 (1934).
16. C. F. Powell. Proc. Roy. Soc. A 119, 553 (1928).
17. N. Gudris and L. Kulikova. Zeit. f. Ph. 25, 121 (1924).